

# Correlated phases of moat-band excitons in two-dimensional systems

L. Maisel Licerán,<sup>1,\*</sup> S. H. Boeve,<sup>1</sup> and H. T. C. Stoof<sup>1</sup>

<sup>1</sup>*Institute for Theoretical Physics and Center for Extreme Matter and Emergent Phenomena,  
Utrecht University, Princetonplein 5, 3584 CC Utrecht, The Netherlands*

(Dated: February 23, 2026)

We study two-dimensional systems of interacting excitons with a moat dispersion, for which the ground-state energy manifold presents a ring of discrete or continuously degenerate minima around a single point in momentum space. At low densities and for an idealized, perfectly degenerate moat, we show that the excitons undergo statistical transmutation and stabilize a chiral spin liquid. At higher densities, the moat dispersion favors Bose–Einstein condensation into states occupying multiple momenta, leading to inhomogeneous condensate phases and potentially supersolidity. We discuss the impact of band-structure warping present in realistic systems and argue that it generically stabilizes Bose-condensed phases over the chiral spin liquid, and analyze the superfluid response of the former which is unconventional due to the moat band. We also demonstrate that a proper renormalization of the exciton–exciton interaction is essential for describing these phases, and show that even purely repulsive interactions can favor inhomogeneous condensates. To further explore inhomogeneous condensate phases, we employ a Gross–Pitaevskii framework with a pseudopotential approximation and map out the resulting phase diagram. We show that the presence of degenerate dispersion minima can drive supersolidity already at weak coupling, in contrast to systems with a standard parabolic dispersion. Finally, we discuss our results in the context of real excitonic systems and argue that moat-band-induced supersolidity can be within experimental reach for realistic values of the model parameters.

## I. INTRODUCTION

Excitons are bound electron–hole pairs in semiconductors that can display bosonic statistics due to their composite fermionic nature. In recent years, two-dimensional (2D) exciton systems have emerged as promising and highly tunable platforms to realize novel correlated many-body phases. Two decades ago, excitonic condensation was first achieved in quantum-Hall bilayers of electrons and holes [1, 2], and more recently the condensation of excitons composed of fractional charges has been realized in similar systems [3]. On the other hand, the rise of highly tunable 2D systems such as stacked (and possibly twisted) transition-metal dichalcogenides has facilitated the experimental realization of correlated phases even in the absence of strong magnetic fields [4–8]. Examples include interlayer exciton superfluids [9, 10], excitonic Mott insulators [11–13], and strongly correlated exciton–electron states [14, 15], among others. Furthermore, theoretical proposals in such systems have expanded the possibilities even further by predicting, for instance, supersolid and Mott-moiré excitons [16–18], topological flat-band excitons [19], and Wigner-crystal excitons [20], to name a few.

Here, we propose dilute 2D excitonic systems with a moat dispersion as a platform for realizing exotic phases of correlated bosonic matter. On a moat band, the low-energy manifold comes in the form of a ring-shaped valley in momentum space containing a highly degenerate continuum of ground states that can drive strong correlations. Such an exotic dispersion could appear for instance in systems where the electron or hole band displays a camelback feature, as two of us demonstrated in Ref. [21] in the context of a band-inverted topological insulator. One intriguing possibility concerning the correlated states

on moat bands is the formation of a Bose–Einstein condensate (BEC) phase of the dilute Wannier–Mott excitons when these can be considered almost ideal bosons. In this regard, the degenerate moat offers the possibility of realizing a coherent state where multiple momenta are simultaneously occupied. This leads to breaking of the translational symmetry and can result in a supersolid, a phase combining the solid-like elastic response to shear stress with the superfluid flow of the BEC [22–25]. While the potential supersolidity of excitons has been investigated before in systems with conventional parabolic bands [26–29], we show here that a moat band can lead to inhomogeneous condensates also in the limit of weak interactions, yields an unusual superfluid response, and leads to a competition with other many-body phases depending on the specific degree of degeneracy of the moat. In this regard, another exciting avenue first studied in Refs. [30–34] for the case of hard-core bosons, is that the high degeneracy of the moat causes statistical transmutation of the excitons. The latter are then described as fermions with a unit flux-quantum attachment which occupy the lowest Landau level corresponding to the emergent effective magnetic field, and essentially realize a chiral spin liquid (CSL) state.

In this work, we present a unified framework to describe many-body phases of excitons on moat bands and obtain related phase diagrams that can guide future experimental realizations of the proposed systems. We highlight how an appropriate  $T$ -matrix renormalization of the bare exciton–exciton interaction is crucial to obtain inhomogeneous states and exemplify this in the case of a simple bilayer potential between dipolar excitons. We also review the theory behind the statistical transmutation of bosons on moat bands and compare the energies of the resulting CSL phases with those of the BECs for the simple bilayer model. We then argue that the phenomenon of band-structure warping, expected to be present in real systems, will typically tend to destabilize the CSL and favor the formation of a (possibly supersolid) BEC, and subsequently

\* l.maiselliceran@uu.nl

use a Gross–Pitaevskii framework to study excitonic super-solids across a larger parameter region. Our findings establish moat-band excitons as an exciting avenue for the exploration of correlated phases and add further interest into highly tunable 2D material platforms for the realization of novel interacting bosonic matter.

This article is organized as follows. In Sec. II we introduce the system and a convenient set of three dimensionless parameters that fully characterizes the problem. In Sec. III we develop the theory behind the BEC and CSL phases, paying particular attention to the  $T$ -matrix renormalization. We compare their energies in the case of a simple bilayer potential and discuss the phenomenon of band-structure warping in real systems. In Sec. IV we study the superfluid response of a homogeneous or inhomogeneous moat-band BEC. In Sec. V we introduce a Gross–Pitaevskii framework for the treatment of inhomogeneous and supersolid phases of excitons within a pseudopotential approximation. In Secs. VI and VII we use this framework to compute the phase diagram of a simplified model for excitonic BECs in one and two dimensions, respectively, and develop an analytical Landau theory that matches the numerical Gross–Pitaevskii results. Finally, in Sec. VIII we conclude our work and give an outlook for further work.

## II. MODELING AND PARAMETERS

We consider a system of  $N$  Wannier excitons in the dilute limit, meaning that the exciton number density  $n$  and the exciton radius  $a_X$  satisfy  $na_X^2 \ll 1$ . In terms of bosonic field operators  $\hat{b}(\mathbf{r})$  and  $\hat{b}^\dagger(\mathbf{r})$  representing the excitons, the Hamiltonian of the system is written as (we set  $\hbar = 1$ )

$$\hat{H} = \int d^2r \hat{b}^\dagger(\mathbf{r}) K(\mathbf{p}) \hat{b}(\mathbf{r}) + \frac{1}{2} \int d^2r d^2r' \hat{b}^\dagger(\mathbf{r}) \hat{b}^\dagger(\mathbf{r}') V(\mathbf{r} - \mathbf{r}') \hat{b}(\mathbf{r}') \hat{b}(\mathbf{r}), \quad (1)$$

where  $K$  is the kinetic-energy operator,  $\mathbf{p} = -i\nabla$  is the momentum operator, and  $V$  is the *bare* exciton–exciton interaction, assumed here to depend only on the distance  $|\mathbf{r} - \mathbf{r}'|$ . As explained below, the bare interaction will have to be appropriately renormalized for the treatment of excitonic BECs.

### A. Moat dispersion

We consider a kinetic energy of the form

$$K(\mathbf{p}) = \frac{a^2}{4b} - a\mathbf{p}^2 + b\mathbf{p}^4, \quad (2)$$

characterized by two parameters  $a$  and  $b$ . When  $a > 0$  the single-particle dispersion reads  $\varepsilon_{\mathbf{k}} = b(k^2 - q_m^2)^2$ , where  $k \equiv |\mathbf{k}|$ . This has the form of a Higgs potential and features a moat in 2D, i.e., a ring-shaped valley with radius  $q_m \equiv \sqrt{a/2b}$ . In the 1D case, the “moat” is simply a pair of minima at  $\pm q_m$ . Our task will be to determine how the presence of a moat band

can influence the phase diagram of the interacting system and to find the many-body ground state. Note that the constant shift in Eq. (2) is such that the kinetic energy vanishes at the moat momentum, so the moat energy barrier is  $\varepsilon_m \equiv \varepsilon_0 = a^2/4b$ . Note that Eq. (2) corresponds to the lowest-order terms in a gradient expansion of a moat-shaped kinetic energy and behaves quartically at large momenta. This is not a problem from the point of view of a proof of principle, but in realistic settings we expect a quadratic behavior at large  $k$ . If desired, one can take a dispersion of the form  $(k - q_m)^2/2M$  instead, which however corresponds to a nonlocal operator in position space. Ultimately, the qualitative (and often quantitative) behavior of the system is mostly the same in any scenario, and we will explicitly point out the few differences when they arise.

### B. Effective interaction

Regarding the bare interaction potential  $V(r)$ , it will be crucial that it is *not* a simple contact interaction. Indeed, in many systems it is expected on physical grounds that the exciton–exciton interaction is relatively long-ranged. For instance, the pair potential between two excitons in the  $s$ -wave ground state in monolayers of conventional semiconductors displays an attractive  $-1/r^6$  behavior at long distances due to the induced dipole–dipole nature of the interaction, while in electron–hole bilayer systems the excitons form permanent dipoles leading to a repulsive  $1/r^3$  behavior at large separations. We thus characterize the exciton–exciton interaction via a potential  $V(r)$  with a characteristic strength  $V_0$  and a characteristic length scale  $r_0$  via

$$V(r) = V_0 v(r/r_0), \quad (3)$$

where the dimensionless function  $v$  will be referred to as the interaction kernel. In momentum space the interaction is written as  $V_{\mathbf{q}} = 2\pi V_0 r_0^2 \mathfrak{h}_0[v](qr_0)$ , where  $\mathfrak{h}_n[f](x) \equiv \int_0^\infty du u f(u) J_n(xu)$  is the order- $n$  Hankel transform of  $f$ . Due to the fast decay expected at large distances, we will assume that the interaction is integrable,  $\int d^2r V(r) < \infty$ , such that the zero-momentum Fourier component  $V_0$  is finite.

In a significant portion of this paper we will be concerned with BEC phases of excitons. For these kinds of many-body states, where the ground-state wave function  $\Psi$  at the mean-field level is given by a product of identical wave functions, it is incorrect to use the bare interaction potential between two particles. Indeed, the latter usually contains an ultraviolet divergence, which does not accurately reflect the fact that in the real many-body system the particles will tend to avoid each other at short distances. Thus, it is expected that this divergence of the bare potential in the full theory is canceled by the suppression of the many-body wave function  $\Psi(\{\mathbf{r}_i\})$  when two of the coordinates come close to each other. To account for this, when dealing with a BEC the bare microscopic interaction potential appearing in Eq. (1) must be replaced by an effective energy-dependent many-body  $T$  matrix accounting for interparticle correlations at short distances [35–38]. Furthermore, it has been previously argued [39–42] that in 2D the

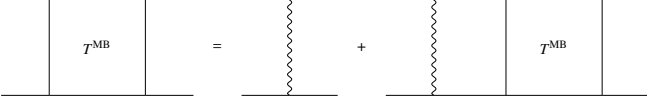


FIG. 1. Diagrammatic Lippmann–Schwinger equation for the many-body  $T$  matrix. The solid lines correspond to many-body propagators and the squiggly lines represent the bare interaction.

many-body  $T$  matrix in a cold Bose gas at low energies must be replaced by the two-body  $T$  matrix at energy  $-2\mu$ , where  $\mu$  is the chemical potential, as this is precisely the energy cost to excite two atoms from the condensate [43]. In Appendix C we show that using the  $T$  matrix is indeed equivalent to including short-range correlations into the many-body wave function.

The many-body  $T$  matrix is diagrammatically given by the ladder sum depicted in Figure 1. The two-body  $T$  matrix can be obtained by replacing the many-body propagators in this diagrammatic Lippmann–Schwinger equation by noninteracting propagators and neglecting the bosonic occupation factors corresponding to the excited states. This leads to

$$T_{kk'}^{2B}(\mathbf{K}, E) = V_{\mathbf{k}-\mathbf{k}'} + \frac{1}{\mathcal{A}} \sum_{\mathbf{p}} V_{\mathbf{k}-\mathbf{p}} \frac{1}{E - \varepsilon_{\mathbf{K}/2+\mathbf{p}} - \varepsilon_{\mathbf{K}/2-\mathbf{p}} + i0^+} T_{\mathbf{p}\mathbf{k}'}^{2B}(\mathbf{K}, E), \quad (4)$$

where  $\mathcal{A}$  is the surface area of the 2D system and the summation can be replaced by an integral in the thermodynamic limit via  $\sum_{\mathbf{p}} \rightarrow \mathcal{A} \int d^2p / (2\pi)^2$ . We see that setting  $E = -2\mu$  results in a fully real  $T$  matrix, so the infinitesimal imaginary part in the denominator can safely be neglected for our purposes. With this definition, the  $T$  matrix enters the second-quantized Hamiltonian as

$$\hat{H}_{\text{int}} = \frac{1}{2\mathcal{A}} \sum_{\mathbf{K}\mathbf{k}\mathbf{k}'} T_{\mathbf{k}\mathbf{k}'}^{2B}(\mathbf{K}, -2\mu) \hat{b}_{\frac{\mathbf{K}}{2}+\mathbf{k}}^\dagger \hat{b}_{\frac{\mathbf{K}}{2}-\mathbf{k}}^\dagger \hat{b}_{\frac{\mathbf{K}}{2}-\mathbf{k}'} \hat{b}_{\frac{\mathbf{K}}{2}+\mathbf{k}'}. \quad (5)$$

This  $\hat{H}_{\text{int}}$  is the correct interaction Hamiltonian to consider when dealing with BECs and is meant to replace the interaction term in the Hamiltonian of Eq. (1) containing the bare interaction. We also note that the bare local interaction  $V_{\mathbf{k}}$  in Eq. (4) may be straightforwardly replaced by a more general, possibly nonlocal bare interaction  $V_{\mathbf{k}\mathbf{k}'}(\mathbf{K})$  depending also on the total momentum  $\mathbf{K}$ . This may be more appropriate if one desires to capture the full detailed behavior of excitonic systems, as it allows for the inclusion of exchange processes taking into account the composite nature of the excitons [44].

### C. Dimensionless parameters

Within our dilute approximation  $na_X^2 \ll 1$  and for  $a > 0$ , i.e., in the presence of a moat, the problem of interacting excitons involves the three length scales  $q_m^{-1}$ ,  $n^{-1/2}$ , and  $r_0$ , and the two energy scales  $\epsilon_m$  and  $V_0$ . By the Buckingham pi theorem, this means that the physics are governed by exactly three dimensionless parameters. Motivated by this observation, we

form the combinations

$$\lambda \equiv -ar_0^2/2b, \quad (6a)$$

$$\rho \equiv \sqrt{\pi n r_0^2}, \quad (6b)$$

$$\gamma \equiv V_0 r_0^4 / b. \quad (6c)$$

Note that these are also well-defined when  $a < 0$ , thus in the absence of a moat. When  $a > 0$ , we can rewrite the first and third in terms of the moat parameters as  $\lambda = -(q_m r_0)^2$  and  $\gamma = (V_0/\epsilon_m)(q_m r_0)^4 = \lambda^2 V_0/\epsilon_m$ . The parameters  $\lambda$  and  $\rho$  compare the range of the interaction with the moat radius and the typical interexciton distance, respectively, while  $\gamma$  describes a competition between the interaction strength and the moat energy barrier and plays the role of an effective interaction strength.

In order to work with these parameters, we make all positions and momenta dimensionless as  $\tilde{\mathbf{r}} \equiv r/r_0$  and  $\tilde{\mathbf{k}} \equiv kr_0$ , respectively (thus in particular  $\tilde{q}_m \equiv q_m r_0$ ), and rescale all energies via  $\tilde{E} = E/(b/r_0^4)$ . Thus, the dimensionless dispersion is  $\tilde{\varepsilon}_{\tilde{\mathbf{k}}} = (\tilde{k}^2 + \lambda)^2$  and the dimensionless interaction in position space is  $\tilde{V}(\tilde{r}) = \gamma v(\tilde{r})$ . We accordingly define the interaction kernel in momentum space as  $v_{\tilde{q}} \equiv \mathfrak{h}_0[v](\tilde{q})$ , and thus the dimensionless interaction in momentum space is  $\tilde{V}_{\tilde{q}} = 2\pi\gamma v_{\tilde{q}}$ . In analogy with  $V_{\mathbf{q}}$ , we define a dimensionless  $T$ -matrix kernel  $t$  via  $T_{\mathbf{k}\mathbf{k}'}^{2B}(\mathbf{K}, E) \equiv 2\pi V_0 r_0^2 t_{\tilde{\mathbf{k}}\tilde{\mathbf{k}'}}(\tilde{\mathbf{K}}, \tilde{E})$ , such that the dimensionless  $T$  matrix is  $\tilde{T}_{\tilde{\mathbf{k}}\tilde{\mathbf{k}'}}^{2B}(\tilde{\mathbf{K}}, \tilde{E}) = 2\pi\gamma t_{\tilde{\mathbf{k}}\tilde{\mathbf{k}'}}(\tilde{\mathbf{K}}, \tilde{E})$ . The equation for the kernel  $t$  reads

$$t_{\tilde{\mathbf{k}}\tilde{\mathbf{k}'}}(\tilde{\mathbf{K}}, \tilde{E}) = v_{\tilde{\mathbf{k}}-\tilde{\mathbf{k}'}} + \frac{2\pi\gamma}{\tilde{\mathcal{A}}} \sum_{\tilde{\mathbf{p}}} \frac{v_{\tilde{\mathbf{k}}-\tilde{\mathbf{p}}} t_{\tilde{\mathbf{p}}\tilde{\mathbf{k}'}}(\tilde{\mathbf{K}}, \tilde{E})}{\tilde{E} - \tilde{\varepsilon}_{\tilde{\mathbf{K}}/2+\tilde{\mathbf{p}}} - \tilde{\varepsilon}_{\tilde{\mathbf{K}}/2-\tilde{\mathbf{p}}}}, \quad (7)$$

where  $\tilde{\mathcal{A}} \equiv \mathcal{A}/r_0^2$  and evidently  $\sum_{\tilde{\mathbf{p}}} \rightarrow \tilde{\mathcal{A}} \int d^2\tilde{p}/(2\pi)^2$  in the thermodynamic limit.

Finally, we note that if the quadratic moat with dispersion  $(k - q_m)^2/2M$  is used, then it becomes more convenient to define  $\lambda \equiv -q_m r_0$  and to measure energies in units of  $(2Mr_0^2)^{-1}$ , so that  $\tilde{\varepsilon}_{\tilde{\mathbf{k}}} = (\tilde{k} + \lambda)^2$  and  $\gamma \equiv 2Mr_0^2 V_0 = (V_0/\epsilon_m)(q_m r_0)^2$ , where now  $\epsilon_m \equiv q_m^2/2M$ .

### III. MANY-BODY PHASES

On an ideal moat band, there is a macroscopically large number of available states. This leads to a phase competition between different kinds of states which we explain in this section. Generally speaking, the results will depend on the specific form of the bare interaction potential  $V(r)$ . However, for concreteness and in order to illustrate the basic physics of the problem, in this section we will consider an electron–hole bilayer system with a simple toy potential modeling the interaction between two excitons, given by

$$V_{XX}(r) = V_0 \left( \frac{1}{r/d} - \frac{1}{\sqrt{1 + (r/d)^2}} \right). \quad (8)$$

Here, the interlayer distance  $d$  plays the role of the  $r_0$  parameter, while  $V_0 \equiv e^2/2\pi\epsilon_0\epsilon_r d$  with  $\epsilon_r$  the effective relative permittivity of the surrounding environment. This pair interaction has

been used before to address interacting exciton problems in bilayer systems [18, 28, 45] and serves as a first approximation to the full interaction motivated by its expected dipole–dipole behavior at large distances. The interaction kernel associated with Eq. (8) is  $v(\vec{r}) = 1/\vec{r} - 1/\sqrt{\vec{r}^2 + 1}$  in position space and  $v_{\vec{q}} = (1 - e^{-\vec{q}})/\vec{q}$  in momentum space.

### A. Bose–Einstein condensates

A well-known phenomenon in a system of bosons at low temperatures is the formation of a BEC. Here we consider the possibility that the excitons condense into a single coherent state populating a finite number of momenta, whose magnitude for weak interactions will be the moat momentum.

Let us first consider a many-body state occupying a single momentum  $\mathbf{g}$  described by the state

$$|\Psi_{\text{FF}}\rangle = \frac{(\hat{b}_{\mathbf{g}}^\dagger)^N}{\sqrt{N!}}|\emptyset\rangle, \quad (9)$$

where  $|\emptyset\rangle$  is the vacuum state containing no excitons. This corresponds to the so-called Fulde–Ferrel (FF) phase [46], which possesses a homogeneous density profile and has vanishing kinetic energy when the magnitude of  $\mathbf{g}$  coincides with the moat momentum  $q_m$ . With this ansatz, the energy per particle of the FF state in the thermodynamic limit is found as

$$\frac{\tilde{E}^{(\text{FF})}}{N} = \tilde{\varepsilon}_{\tilde{\mathbf{g}}} + \rho^2 \gamma t_{\mathbf{00}}(2\tilde{\mathbf{g}}, -2\tilde{\mu}), \quad (10)$$

where in particular the interaction energy has been obtained via the Hamiltonian of Eq. (5). Due to the rotational symmetry,  $t_{\mathbf{00}}(2\tilde{\mathbf{g}}, -2\tilde{\mu})$  only depends on the magnitude of the ordering momentum, so we take  $\tilde{\mathbf{g}} = \tilde{g}\hat{\mathbf{x}}$  without loss of generality and write  $t_{\mathbf{00}}(2\tilde{g}, -2\tilde{\mu})$  henceforth. Using the definition of the chemical potential  $\mu = (\partial E/\partial N)_{\mathcal{A}}$ , and also minimizing the total energy with respect to the ordering momentum  $\tilde{g}$ , we find the coupled equations

$$\tilde{\mu}_{\text{FF}} = \tilde{\varepsilon}_{\tilde{\mathbf{g}}} + 2\rho^2 \gamma t_{\mathbf{00}}(2\tilde{g}, -2\tilde{\mu}_{\text{FF}}), \quad (11a)$$

$$0 = \frac{\partial \tilde{\varepsilon}_{\tilde{\mathbf{g}}}}{\partial \tilde{g}} + \rho^2 \gamma \frac{\partial}{\partial \tilde{g}} t_{\mathbf{00}}(2\tilde{g}, -2\tilde{\mu}_{\text{FF}}). \quad (11b)$$

These must be solved self-consistently for  $\tilde{\mu}$  and  $\tilde{g}$ . In practice, we have found numerically that  $g \approx q_m$  to very good approximation for all combinations of the three dimensionless parameters that determine the behavior of the system, so we use this approximation to speed up the numerical calculations in the FF phase. In this approximation the FF state has zero kinetic energy, and thus the interaction part of Eq. (10) also coincides with the total energy.

We can also consider many-body phases where more than one momentum state is populated. Here we focus on the simplest one, the so-called Larkin–Ovchinnikov (LO) or stripe phase, consisting of a coherent superposition of states with momenta  $\mathbf{g}$  and  $-\mathbf{g}$  described by [47]

$$|\Psi_{\text{LO}}\rangle = \frac{1}{\sqrt{N!}} \left( \frac{e^{i\theta} \hat{b}_{\mathbf{g}}^\dagger + e^{-i\theta} \hat{b}_{-\mathbf{g}}^\dagger}{\sqrt{2}} \right)^N |\emptyset\rangle, \quad (12)$$

where  $\theta$  is an arbitrary phase [48]. More generally, one should also include the components  $0, \pm 2\mathbf{g}, \pm 3\mathbf{g}, \dots$ , but we focus here on the simplest case for simplicity. In this case the interaction energy per particle reads

$$\frac{\tilde{E}^{(\text{LO})}}{N} = \tilde{\varepsilon}_{\tilde{\mathbf{g}}} + \rho^2 \gamma t_{\text{eff}}^{(\text{LO})}(\tilde{\mathbf{g}}), \quad (13)$$

where for convenience we have defined

$$\begin{aligned} t_{\text{eff}}^{(\text{LO})}(\tilde{\mathbf{g}}) &\equiv \frac{1}{2} \left[ t_{\mathbf{00}}(2\tilde{\mathbf{g}}, -2\tilde{\mu}_{\text{LO}}) + t_{\tilde{\mathbf{g}}\tilde{\mathbf{g}}}(\mathbf{0}, -2\tilde{\mu}_{\text{LO}}) + t_{\tilde{\mathbf{g}}, -\tilde{\mathbf{g}}}(\mathbf{0}, -2\tilde{\mu}_{\text{LO}}) \right]. \end{aligned} \quad (14)$$

As before, we are allowed to take  $\tilde{\mathbf{g}}$  along an arbitrary direction, say the  $x$  axis, so we write  $t_{\text{eff}}^{(\text{LO})}(\tilde{g})$  in what follows. That the energy of Eq. (13) is independent of  $\theta$  can be understood from the fact that the wave function is proportional to  $\cos(\mathbf{g} \cdot \mathbf{r} + \theta)$ , and thus a change in  $\theta$  is equivalent to the sliding of the coordinate-space density pattern that defines one of the two zero-energy Goldstone modes. Similarly to the FF case, the chemical potential and the magnitude of the ordering momentum must be found self-consistently by solving the coupled equations

$$\tilde{\mu}_{\text{LO}} = \tilde{\varepsilon}_{\tilde{\mathbf{g}}} + 2\rho^2 \gamma t_{\text{eff}}^{(\text{LO})}(\tilde{g}), \quad (15a)$$

$$0 = \frac{\partial \tilde{\varepsilon}_{\tilde{\mathbf{g}}}}{\partial \tilde{g}} + \rho^2 \gamma \frac{\partial}{\partial \tilde{g}} t_{\text{eff}}^{(\text{LO})}(\tilde{g}). \quad (15b)$$

For the numerical results of this section we focus on the case when the parameter  $\Lambda \equiv 2\rho^2 \gamma$  is kept fixed with  $\Lambda \ll 1$ , as in this case we can take  $\tilde{g} \approx \tilde{q}_m$  for both phases. This simplifies the problem as it allows us to solve a single self-consistent equation for the chemical potential in each phase, namely Eqs. (11a) and (15a), as Eqs. (11b) and (15b) are approximately satisfied since  $\partial \tilde{\varepsilon}_{\tilde{\mathbf{g}}}/\partial \tilde{g} = 0$  at the moat momentum. This parameter  $\Lambda$  plays a similar role to the well-known diluteness parameter of the physics of cold atoms. However, its physical interpretation in our case is not as straightforward as it contains both the dimensionless density  $\rho$ , measuring the true diluteness of the system, as well as the dimensionless coupling constant  $\gamma$ . It thus represents a competition between the system diluteness and the relative interaction strength and can in principle assume a broad range of values compared to its cold-atom counterpart.

In Figure 2 we show plots of the energy difference between the FF and LO phases on the  $\tilde{q}_m$ - $\gamma$  plane for both a quadratic moat and a quartic moat (we recall the relations  $\lambda = -\tilde{q}_m$  for the former and  $\lambda = -\tilde{q}_m^2$  for the latter). The value of  $\rho$  is appropriately chosen at each point so as to keep  $\Lambda \ll 1$  fixed. The results show that the inhomogeneous stripe phase can have lower energy than the FF phase in a large region of the parameter space, and it can be seen that a large moat favors the formation of an inhomogeneous BEC even in the case of weak interactions, i.e.,  $V_0/\epsilon_m = \gamma/\lambda^2 \ll 1$ . The renormalization of the bare interaction via the  $T$  matrix, whose

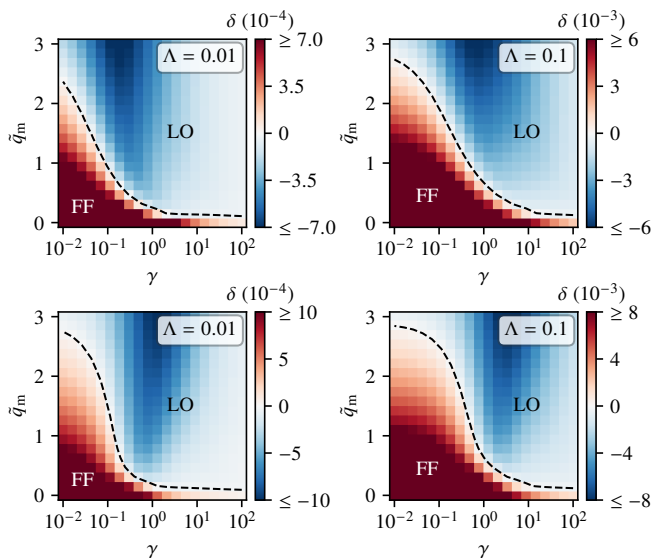


FIG. 2. Energy difference  $\delta \equiv (\bar{E}^{(\text{LO})} - \bar{E}^{(\text{FF})})/N$  on the  $\tilde{q}_m$ - $\gamma$  plane for a quadratic moat (top) and a quartic one (bottom) for two different values of the small fixed parameter  $\Lambda \equiv 2\rho^2\gamma$ . In this regime, the ordering vector has the magnitude of the moat momentum and the two phases have vanishing kinetic energy, so the energies coincide with the interaction energies. The dashed black line marks the phase boundary between the homogeneous and inhomogeneous phases. As  $\rho = \sqrt{\Lambda/2\gamma}$ , one observes that a smaller  $\rho$  favors the formation of an LO phase at fixed  $\tilde{q}_m$  and  $\gamma$ , as the transition line shifts to smaller  $\gamma$  and smaller  $\tilde{q}_m$ . The calculation takes into account the full  $T$  matrix associated with the bilayer exciton-exciton potential of Eq. (8) and shows that the existence of a moat can give rise to translationally broken phases even in the case of weak interactions and dilute exciton densities.

numerical treatment is explained in Appendix C, is crucial for these results. Indeed, the bare momentum-space interaction  $V_{\mathbf{k}}$  is positive everywhere, and thus by itself cannot lead to a stable LO phase or any other inhomogeneous phase [49, 50]. This is also clear from Eqs. (10) and (14) if we replace the full kernel  $t_{\mathbf{k}\mathbf{k}'}(\mathbf{K}, -2\tilde{\mu})$  by a local, energy-independent function  $t_{\mathbf{k}-\mathbf{k}'}$  in this case.

For completeness we have also checked the possibility of a hybrid LO state with a nonzero zero-momentum component, i.e.,

$$|\Psi_{\text{HLO}}\rangle = \frac{1}{\sqrt{N!}} [c_0 \hat{b}_0^\dagger + c_g (\hat{b}_g^\dagger + \hat{b}_{-g}^\dagger)]^N |\emptyset\rangle, \quad (16)$$

where  $|c_0|^2 + 2|c_g|^2 = 1$ . In principle, this state could develop continuously from the LO phase by developing a small nonzero  $c_0$  and would display the superfluid properties associated with a homogeneous BEC besides also exhibiting a periodic density pattern (cf. Sec. IV). By expanding the free energy for an infinitesimal  $c_0$  as explained in Appendix B, we however conclude that this always results in a positive energy difference with respect to the pure LO state and is thus disfavored.

Even though in this section we have focused specifically on the comparison between the FF and LO phases, higher-order inhomogeneous BECs, i.e., coherent states formed by a super-

position of more than two momenta, can be considered as well. Their general treatment is outlined in Appendix B. In particular, in our numerics we have also considered phases for which the coherent wave function for  $\Lambda \ll 1$  consists of a superposition of three momenta on the moat, whose position-space density profile is then a triangular lattice. Its self-consistent equations are identical to Eqs. (15a)–(15b) with the effective kernel replaced by

$$t_{\text{eff}}^{(\Delta)}(\tilde{g}) \equiv \frac{1}{3} \left[ t_{00}(2\tilde{g}\hat{x}, -2\tilde{\mu}_\Delta) + 2t_{\frac{\sqrt{3}}{2}\tilde{g}\hat{y}, \frac{\sqrt{3}}{2}\tilde{g}\hat{y}}(\tilde{g}\hat{x}, -2\tilde{\mu}_\Delta) + 2t_{\frac{\sqrt{3}}{2}\tilde{g}\hat{y}, -\frac{\sqrt{3}}{2}\tilde{g}\hat{y}}(\tilde{g}\hat{x}, -2\tilde{\mu}_\Delta) \right]. \quad (17)$$

We find that, for  $\gamma \ll 1$ , this phase is stabilized at around  $\tilde{q}_m \sim 5.5$ – $5.9$  for both the quadratic and quartic moats (note that this is not shown in the parameter region of Fig. 2). Despite the fact that it breaks the translational symmetry, such a triangular phase can exhibit superfluid flow and is therefore called a supersolid. The superfluid response of these different inhomogeneous BECs is analyzed in detail in Sec. IV.

States where the condensate wave function populates a higher number of momenta can also be considered, and the interaction energy and the self-consistent equations they satisfy can be found by following the methods described in this section. In this article, these states will be explored in a later section by means of the aforementioned pseudopotential approximation in order to speed up the numerical calculations. Another intriguing possibility is that of a fragmented condensate, which has been predicted in some systems with a moat band where the renormalized interaction acquires a strong angular dependence [51, 52]. As an example, we have computed the energy for a fragmented condensate with wave function

$$|\Psi_{\text{FBEC}}\rangle = \frac{(b_g^\dagger)^{N/2} (b_{-g}^\dagger)^{N/2}}{\sqrt{(N/2)!} \sqrt{(N/2)!}} |\emptyset\rangle, \quad (18)$$

but have found the same interaction energy in terms of the  $T$  matrix as for the LO phase. In a finite system, true spontaneous symmetry breaking into a coherent condensate phase is not possible and the system will tend to fragment, which corresponds to similar physics as those of the phase-diffusion problem [53]. Meanwhile, the states  $|\Psi_{\text{LO}}\rangle$  and  $|\Psi_{\text{FBEC}}\rangle$  are in principle degenerate in the thermodynamic limit, but we expect that small spatial inhomogeneities will tend to phase lock the fragmented condensate and give rise to the stripe phase [54]. For this reason we do not consider these kinds of fragmented states in the remainder of the article.

## B. Composite fermion states

While the picture of many-body phases of bosons in first instance naturally leads one to think of Bose-Einstein condensation, another intriguing possibility arises in the case of a moat band. Namely, as studied in Refs. [30–34, 55], the bosons may undergo statistical transmutation into a many-body ground state of effective composite fermions. The fact

that a moat band can cause this effect can intuitively be understood from the fact that such a band exhibits a macroscopic degeneracy, which is reminiscent of the Landau levels (LLs) in the quantum Hall effect (QHE). As shown explicitly below, we can view the bosons as fermions with a unit flux-quantum attachment generating an effective magnetic field. Then, at low enough densities, the emergent fermions can populate appropriate LLs and perfectly quench their mean-field kinetic energy due to the familiar quantum-Hall physics. With both the BEC phases and the composite fermion phases having vanishing kinetic energy, the correlation energy becomes the important point of comparison between both families of states. The aforementioned articles exclusively consider hard-core bosons, i.e., bosons interacting with a repulsive delta-function potential. In this scenario, it is clear that such a composite state of fermions will have the lowest energy at the mean-field level, because the interaction energy must vanish in the case of a contact interaction due to the Pauli exclusion principle. However, as we have argued, excitons generally do not exhibit such a short-ranged interaction, and thus we expect an interesting competition between the correlation energies which we explore in this section and the next one.

Let us first show explicitly how to derive the fermionization of bosons. Starting from the bosonic Hamiltonian of Eq. (1), we perform a flux-attachment transformation for the excitons given by [56–58]

$$\hat{b}(\mathbf{r}) = \hat{f}(\mathbf{r}) \exp \left\{ i \int d^2 r' \arg(\mathbf{r} - \mathbf{r}') \hat{n}(\mathbf{r}') \right\}, \quad (19)$$

where  $\arg(\mathbf{r} - \mathbf{r}')$  is the angle sustained by the vector connecting the points  $\mathbf{r}$  and  $\mathbf{r}'$  as measured from some reference direction, say the  $x$  axis. With this definition, the field operator  $\hat{f}(\mathbf{r})$  replacing the excitons obeys fermionic anticommutation relations. This transformation introduces a statistical Chern–Simons gauge field in the kinetic term via  $\mathbf{p} \rightarrow \mathbf{p} - \hat{\mathbf{a}}$ , with

$$\hat{\mathbf{a}}(\mathbf{r}) = \int d^2 r' \frac{\hat{\mathbf{z}} \times (\mathbf{r} - \mathbf{r}')}{|\mathbf{r} - \mathbf{r}'|^2} \hat{n}(\mathbf{r}'). \quad (20)$$

Thus,  $(\nabla \times \hat{\mathbf{a}}(\mathbf{r}))_z = 2\pi \hat{n}(\mathbf{r})$  is an effective magnetic field experienced by the emergent fermions. At the mean-field level we replace  $\hat{n}(\mathbf{r})$  with an average homogeneous density  $n$ , thus essentially “smearing” the magnetic flux equally over all particles in the system. In this way we obtain the energy of the emergent LLs (in dimensionless units) as

$$\tilde{E}_{\text{LL}}^{(l)} = [2(2l+1)\rho^2 + \lambda]^2, \quad l = 0, 1, 2, \dots \quad (21)$$

for the quartic moat. These LLs are depicted in Fig. 3 as a function of  $\rho$  for a fixed value of  $q_m$ . It is important to note that, contrary to the usual QHE in a system with parabolic bands, the lowest Landau level (LLL) is not always that with  $l = 0$ , but instead depends on density and moat size. We see that the kinetic energy is perfectly quenched at the densities

$$n_l = \frac{q_m^2}{2\pi(2l+1)}. \quad (22)$$

In the fermionized picture, the ground state of the system at density  $n_l$  will be that of a fully filled LL with index  $l$ , which

will be the LLL at this density. The bosonic many-body wave function of this state is then constructed as [34]

$$\Psi_{\text{B}}^{(l)}(\{z_i, \bar{z}_i\}) = \prod_{i < j}^N \frac{z_i - z_j}{|z_i - z_j|} \Psi_{\text{F}}^{(l)}(\{z_i, \bar{z}_i\}), \quad (23)$$

where  $z_i = x_i + iy_i$  is the 2D coordinate of the  $i$ th fermion and  $\Psi_{\text{F}}^{(l)}$  is a Slater determinant of the single-particle wave functions corresponding to the fully filled LLL. In symmetric gauge  $\mathbf{a}(\mathbf{r}) = \pi n(-y, x, 0)$ , the single-particle wave functions adopt the usual forms involving Laguerre polynomials. The wave function of Eq. (23) describes a chiral spin liquid (CSL) and corresponds to a phase where all momenta on the moat are simultaneously occupied and no condensation occurs [31]. Moreover, when the average density  $n$  is not exactly equal to one of the  $n_l$ , but rather  $n_{l+1} < n < n_l$ , the system may undergo phase separation into two such CSL phases with densities  $n_{l+1}$  and  $n_l$ , in such a way that  $n = \alpha n_l + (1 - \alpha)n_{l+1}$  where  $\alpha$  is the volume fraction occupied by the phase with density  $n_l$ .

When the (spinless) bosons interact with a Dirac-delta potential  $V_0 \delta(\mathbf{r})$ , the flux-attachment procedure leads to a system of noninteracting fermions due to the Pauli exclusion principle. However, when the interaction is somewhat long-ranged, the correlation energy will not vanish. Instead, in the case of the bilayer potential it will be given by

$$\frac{\tilde{E}_{\text{int}}^{(l=0)}}{N} = \rho^2 \gamma - \frac{\sqrt{\pi}}{2} \rho \gamma (1 - e^{\rho^2} \text{erfc } \rho) \quad (24)$$

for fermionized bosons in the  $l = 0$  LL. The derivation of Eq. (24) can be found in Appendix D, where we also give a formal expression for the interaction energy of LLs with  $l > 0$ . For the CSL state, the kinetic energy will be nonzero whenever  $\rho > q_m^2/2\pi$ , in which case there will be an additional contribution of  $(2\rho^2 + \lambda)^2$  per particle due to the LL energy.

### C. Phase competition

We are now in the position to compare the energies of the CSL and BEC phases. The interaction energy of the CSL state for small  $\rho$  behaves as  $\rho^3$ , thus as  $n^{3/2}$ . This can be seen by expanding Eq. (24), but it can be rigorously shown for all  $l$  as explained in Appendix D. Thus, for small densities and at the mean-field level, the CSL state is more energetically favorable than any BEC. Indeed, as can be seen for instance from Eqs. (10) and (13), the interaction energy of a BEC phase scales linearly with  $n$  at all densities (insofar as the dilute limit  $na_X^2 \ll 1$  is satisfied) as long as we assume that the  $T$  matrix only has a weak dependence on  $\rho$ . In fact, we numerically find that the interaction energy of the CSL is always lower than that of the FF phase, even at high densities. However, the FF state always has almost vanishing kinetic energy, while the “kinetic energy” of the CSL state can only be fully quenched as long as  $n < q_m^2/2\pi$ . This leads to a transition from the CSL to the FF phase (and by extension also to inhomogeneous BEC phases) as a function of the density. In Fig. 3 we present the phase diagram in the  $n$ - $d$  plane for the bilayer model in an

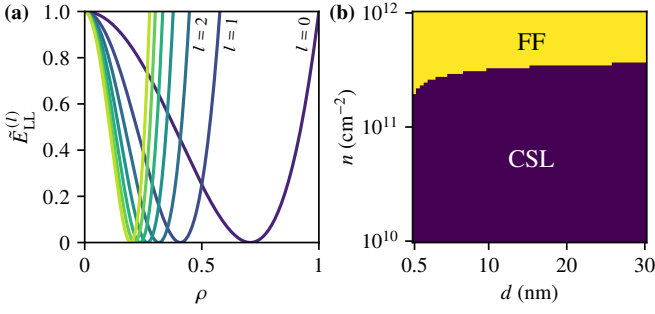


FIG. 3. (a) Landau levels  $\tilde{E}_{LL}^{(l)} = [2(2l + 1)\rho^2 + \lambda]^2$  as a function of the density parameter  $\rho$  for  $\lambda = -1$  and various values of  $l$ . Below  $\rho = \sqrt{-\lambda/2} \approx 0.707$ , the system can always perfectly quench the mean-field kinetic energy by distributing particles between two adjacent levels. This is not possible when  $\rho$  is larger than this value, and the kinetic energy of the system will increase with the density. (b) Phase diagram in the  $n$ - $d$  plane showing the competition between the Fulde-Ferrel phase corresponding to a homogeneous Bose-Einstein condensate and the chiral spin liquid phase of fermionized excitons in a bilayer system with the exciton-exciton interaction of Eq. (8). As a result of the eventual increase of the kinetic energy with the density, at large  $n$  the chiral spin liquid disappears in favor of the condensate at a single momentum on the moat. We have used the experimentally reasonable values  $q_m = 0.1 \text{ nm}^{-1}$ ,  $\epsilon_m = 10 \text{ meV}$ , and  $\epsilon_r = 12$  for the relative permittivity of the surrounding medium.

experimentally sensible range. While the details of the phase diagram will depend on the specific form of the interaction and single-particle dispersion, the qualitative behavior described above is expected for an arbitrary long-range interaction. We stress that this plot is only a comparison between the CSL and the FF phases, and we have not considered inhomogeneous BEC phases such as the LO state described in the previous section. While these could in principle replace the FF phase at the top right corner of the diagram, they will not significantly affect the region where the CSL is present.

Let us briefly comment on the situation with a true contact interaction. The interaction energy of the CSL state in this case vanishes identically, and one would assume that the FF state always has a higher energy. While this is true at the mean-field level, it turns out that fluctuations can stabilize the FF state in a region of the parameter space, as explained in Refs. [33, 34]. This can be intuitively understood from the fact that the CSL state does not truly have zero kinetic energy; the latter is only perfectly quenched at the mean-field level where the statistical magnetic field has been set to a constant. By contrast, when  $\hat{\mathbf{a}}$  is allowed to fluctuate, there can be a transition to the FF state even in the case of a point interaction. More precisely, for a fixed density, the CSL is stable at large coupling while the FF state becomes favorable at small coupling. As this is already the trend that our long-range calculation reveals (because in our case the coupling is inversely proportional to the interlayer distance), we do not expect fluctuations to result in significant qualitative changes to the phase diagram of Fig. 3.

#### D. The role of band-structure warping

In the previous sections we have assumed an ideal moat, i.e., one where all states are perfectly degenerate, and have seen that this favors the CSL phase at low densities, with the FF phase overtaking at higher densities. From our theory so far, and in agreement with the existing literature, it would seem that larger moats increasingly favor the CSL phase, as the LLs of Fig. 3 get shifted to the right with increasing  $q_m$  and the density necessary to reach the  $l = 0$  level becomes higher. However, in real systems where one would hope to observe such excitonic many-body states, another effect is present which will tend to spoil the perfect degeneracy of the moat at large  $q_m$ , namely band-structure warping due to the effects of the underlying crystal lattice [59].

Typically, the low-energy effective model for electrons and holes is written as a  $\mathbf{k} \cdot \mathbf{p}$  expansion up to quadratic order in  $\mathbf{k}$ . This often results in dispersions with perfect rotational symmetry. However, including higher-order terms almost always spoils this symmetry and produces effects reflecting the point-group symmetries of the underlying lattice. For instance, in Ref. [21] we considered excitons in a Bernevig-Hughes-Zhang model for a topological insulator with a band inversion. The latter results in an inverted particle-hole continuum, which in turn results in a moat dispersion for the excitons. While this is a good approximation to obtain the behavior of the free excitons, we must be careful when making assumptions about the many-body behavior of the system that rely on the perfect degeneracy of the emerging moat.

In this case, the physical crystal under consideration has a  $C_3$  rotational symmetry. Following Ref. [60], we include in the  $\mathbf{k} \cdot \mathbf{p}$  model terms cubic in the momenta  $k_x$  and  $k_y$ . By projecting the resulting Hamiltonian on the first set of bulk bands as described in our Ref. [21] we obtain the effective Hamiltonian to be used for the exciton calculation, now up to order  $k^3$ . In order to analyze the effects of such warping terms we obtain the particle-hole continuum in the cubic model by minimizing the electron-hole gap  $\epsilon_{\mathbf{K}/2+\mathbf{k}}^c - \epsilon_{\mathbf{K}/2-\mathbf{k}}^v$  for fixed total exciton momentum  $\mathbf{K}$ . Note that, while this is not the actual exciton energy, we expect a very similar splitting for the latter as the excitons will tend to follow the continuum. The result is plotted in Fig. 4 and shows that the warping terms lead to the lifting of the moat degeneracy into six equal minima separated by an angle of  $\pi/3$ , resulting in a finite effective mass in the direction tangential to the moat. In general, if the dispersion shows  $N_{\min}$  degenerate minima separated by a small energy barrier  $\delta\epsilon$ , this tangential effective mass can be estimated as

$$m_{\text{eff}}^{\parallel} \sim \left( \frac{\pi}{N_{\min}} \right)^2 \frac{q_m^2}{2\delta\epsilon}. \quad (25)$$

For realistic values of the parameters governing the warping perturbation, we find that the energy barrier separating the different minima of Fig. 4 is of the order of a few meV. This corresponds to a few tens of Kelvin, meaning that the warping perturbation in this and similar systems should be enough to lock the bosons into the minima at low enough temperatures.

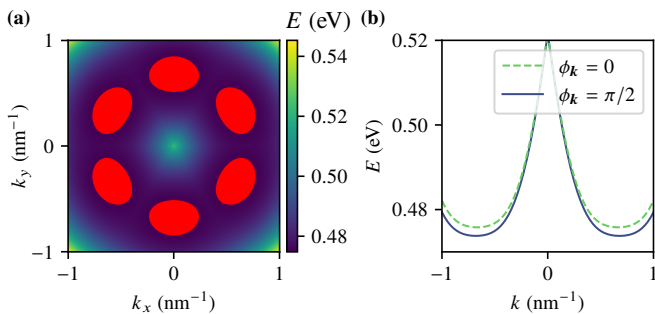


FIG. 4. (a) Particle-hole continuum of the bulk-projected Bernevig–Hughes–Zhang model for bismuth selenide of Ref. [60] in the presence of hexagonal warping. The projection onto the low-energy bulk bands follows the procedure of Ref. [21], and we use the same numerical values for the parameters. Due to cubic terms in  $k_x$  and  $k_y$ , the dispersion reflects the  $C_3$  symmetry of the underlying lattice, breaking the perfect rotational symmetry of the quadratic model and featuring six minima around the  $\Gamma$  point. The red blobs mark regions that differ from the minimum by at most 1 meV. (b) Horizontal and vertical slices of the dispersion in (a) showing the energy in the  $k_x$  and  $k_y$  directions, which contain the largest and smallest minima. The maximum splitting between the two dispersions is about 2 meV (corresponding to approximately 23.2 K) for realistic warping parameters  $R_1 = 0.05 \text{ eV nm}^3$  and  $R_2 = -0.1 \text{ eV nm}^3$  (cf. Ref. [60]).

The effect of warping becomes more significant at momenta away from the  $\Gamma$  point, meaning it will be more important for larger moats. Consequently, for relatively large moats we expect a return from the CSL to the BEC phases as the warping becomes more pronounced. This is because the CSL phase hinges on the simultaneous occupation of all moat momenta and will be significantly affected by the appearance of inhomogeneities in the moat energy landscape. On the other hand, BEC phases only require a discrete number of occupied momenta and are thus almost unaffected by the warping as long as their discrete rotational symmetry is compatible with that of the ground-state dispersion. Furthermore, the presence of energy barriers between the discrete minima not only tends to favor condensation, but also plays the role of weakening the effects of fluctuations. As explained in Refs. [33, 61], on a perfectly degenerate moat these may destabilize the BEC due to the 1D-like divergence of the density of states, a problem that becomes less severe under the effects of warping. Thus, if warping is assumed to be significant, then the phase diagrams of Fig. 2 remain valid as the CSL state becomes energetically unfavorable due to a macroscopic number of excitons occupying the relative maxima along the moat contour.

#### IV. SUPERFLUID RESPONSE ON MOAT BANDS

A natural question regarding the condensate solutions we have found is whether these configurations can exhibit superfluid flow and how the latter is affected by the moat band compared to the parabolic case. The superfluid response of a system can be quantified by the superfluid stiffness  $\mathbf{D}_s$ , a tensor measuring the rigidity of the coherent many-body phase

responsible for the existence of a nondissipative flow. By considering an overall phase difference  $(\Delta\varphi)_i$  applied over the system in direction  $i$ , the components of  $\mathbf{D}_s$  are obtained from the quadratic part of the energy shift via

$$D_s^{ij} = \left. \frac{\partial^2 E[\varphi_{\min}]}{\partial(\Delta\varphi)_i \partial(\Delta\varphi)_j} \right|_{\Delta\varphi=0}. \quad (26)$$

Here,  $E[\varphi_{\min}]$  is the energy corresponding to the many-body configuration  $\Psi_\varphi(\mathbf{r}) \equiv e^{i\varphi(\mathbf{r})}\Psi_0(\mathbf{r})$  when the phase is chosen as  $\varphi_{\min}(\mathbf{r})$ , i.e., the phase profile that minimizes the energy functional under the boundary conditions imposed by the external phase difference, and  $\Psi_0(\mathbf{r})$  is the (phase-independent) macroscopic wave function defining the density profile.

A nontrivial phase profile only affects the kinetic energy, which now reads

$$K[\varphi] = b \int d^2r |(\mathbf{p}^2 - q_m^2)\Psi_\varphi(\mathbf{r})|^2. \quad (27)$$

We will focus on the case  $\Lambda \ll 1$ , so that  $\Psi(\mathbf{r})$  can be taken as a linear superposition of plane waves with momenta distributed along the moat. Explicitly, this means that

$$\Psi_0(\mathbf{r}) = \sqrt{n} \sum_i c_i e^{i\mathbf{q}_i \cdot \mathbf{r}}, \quad (28)$$

where  $|\mathbf{q}_i| \approx q_m$  for all  $i$  and  $\sum_i |c_i|^2 = 1$ .

We assume the long-wavelength limit for the phase  $\varphi$ , meaning that the latter varies over distances much larger than the characteristic moat length  $L_m \sim 1/q_m$  which defines the period of the position-space density pattern,  $L_m \ll L_{\Delta\varphi}$ . In this long-wavelength limit, the action of the operator appearing in Eq. (27) on a plane wave making up the condensate wave function  $\Psi$  can be approximated as

$$(\mathbf{p}^2 - q_m^2)e^{i\mathbf{q} \cdot \mathbf{r} + i\varphi(\mathbf{r})} \approx 2(\mathbf{q} \cdot \nabla\varphi)e^{i\mathbf{q} \cdot \mathbf{r} + i\varphi(\mathbf{r})}, \quad (29)$$

where we have neglected terms quadratic in the phase gradient as these are slowly varying. From Eq. (29) we see that the superfluid behavior in the presence of a moat band will contain fundamental differences with respect to the parabolic case. Indeed, the latter simply gives  $n(\mathbf{r})(\nabla\varphi)^2$  for the part quadratic in the phase gradient. Meanwhile, the energy functional in the moat-band case depends on  $|\sum_i (\mathbf{q}_i \cdot \nabla\varphi)e^{i\mathbf{q}_i \cdot \mathbf{r} + i\varphi}|^2$ , which couples the different momenta to the components of  $\nabla\varphi$ . As a result, we expect a strongly anisotropic superfluid stiffness tensor and nonzero off-diagonal components in triangular and higher-order supersolids.

We are now in the position to compute the superfluid stiffness for various BEC phases. To this end, we must firstly solve the equation of motion for  $\varphi$  that minimizes Eq. (27) and compute the resulting expression for  $\Delta E$ . We begin with the FF phase, thus  $\Psi_{\text{FF}}(\mathbf{r}) = \sqrt{n}e^{i\mathbf{q} \cdot \mathbf{r} + i\varphi(\mathbf{r})}$  by orienting the  $x$  axis of our coordinate system along the symmetry-breaking direction. The equation of motion trivially reads  $\partial_x^2 \varphi = 0$ , so that  $\partial_x \varphi = (\Delta\varphi)_x/L$ . This results in the energy shift

$$K_{\text{FF}} = \frac{1}{2}(8bq_m^2n)(\Delta\varphi)_x^2, \quad (30)$$

from where we read off  $D_{s,FF}^{xx} = 8bq_m^2$  and all other components are zero. This result implies that the phase stiffness is nonzero in the longitudinal direction and vanishes in the transverse direction relative to the ordering vector  $\mathbf{q}$ . This is to be expected, as for a perfectly degenerate moat there can only be phase stiffness in the direction perpendicular to the moat, and in fact the obtained  $D_{s,FF}^{xx}$  corresponds exactly to the familiar result  $n/m_{\text{eff}}^{xx}$  with  $1/m_{\text{eff}}^{xx} = 8bq_m^2$  the inverse effective mass in the radial direction. By contrast, the flatness of the moat in the tangential direction causes the stiffness to vanish.

The fact that only  $D_{s,FF}^{xx}$  is nonzero for a perfectly degenerate moat is expected to have significant consequences at nonzero temperatures. Indeed, the Berezinskii-Kosterlitz-Thouless (BKT) temperature is given by  $k_B T_{\text{BKT}} = \frac{\pi}{2} \sqrt{\det D_s}$ , where the determinant of the superfluid stiffness tensor vanishes in the FF phase. This implies that the FF phase cannot exist at nonzero temperatures in the presence of a perfect moat degeneracy. Once the degeneracy is lifted via, for instance, the warping mechanism explained previously, this issue disappears and we expect a phase transition at nonzero temperatures.

For the FF case, this will be  $k_B T_{\text{BKT}} = n\pi/2 \sqrt{m_{\text{eff}}^{xx} m_{\text{eff}}^{yy}}$ , where  $m_{\text{eff}}^{yy}$  is the effective mass in the direction tangential to the moat estimated in Eq. (25).

Next we turn to the LO phase, which features two plane waves with momenta which we choose to lie at  $\pm q_m \hat{\mathbf{x}}$ . The equation of motion for the phase [for a suitable choice of the arbitrary phase  $\theta$  appearing in Eq. (12)] reads  $\partial_x (\cos^2 q_m x \partial_x \varphi) = 0$ , hence  $\partial_x \varphi = C(\Delta\varphi)_x / \cos^2 q_m x$  with  $C \equiv (\int_0^L dx / \cos^2 q_m x)^{-1}$ . Plugging this into the expression for the energy reveals that  $D_{s,LO}^{xx} \propto C$ , which vanishes, so there is no superfluidity in the LO phase. That the superfluid stiffness must vanish for the LO phase can also be understood from Leggett's bound on the superfluid fraction  $f_s \equiv n_s/n$ , which states that [24, 62]

$$f_s \leq \frac{1}{n} \left\langle \frac{1}{\langle n(\mathbf{r})^{-1} \rangle_{\hat{\mathbf{e}}_1}} \right\rangle_{\hat{\mathbf{e}}_2}, \quad (31)$$

where  $\hat{\mathbf{e}}_1$  and  $\hat{\mathbf{e}}_2$  are orthogonal directions and  $\langle \dots \rangle_{\hat{\mathbf{e}}_i}$  stands for the spatial average over each of them [63]. The vanishing of  $D_s$  for the stripe phase can be understood intuitively, because the density pattern exhibits entire lines where  $n(\mathbf{r})$  vanishes. On these lines it is possible to perform a finite phase slip at no additional energy cost, so that adjacent stripes are not phase-coherent.

In the triangle phase, the equation of motion for the phase profile cannot be solved analytically. Instead, we perform a variational calculation to bound the eigenvalues of the superfluid stiffness tensor. To this end we must take into account the orientation  $\theta$  of one of the momentum basis vectors with respect to the axes of the physical sample. Defining  $\mathbf{r}(\theta) = \mathbf{R}(\theta)\mathbf{r}$ , with  $\mathbf{R}(\theta)$  the 2D rotation matrix with angle  $\theta$ , the kinetic energy in the long-wavelength limit reads

$$K_\Delta = 4bq_m^2 n \int d^2r (\nabla\varphi)^\top \mathbf{F}(\mathbf{r}(\theta), \theta) (\nabla\varphi), \quad (32)$$

where  $\mathbf{F}(\mathbf{r}(\theta), \theta) = \mathbf{R}(\theta)^\top \mathbf{F}(\mathbf{r}(\theta), 0) \mathbf{R}(\theta)$  with the compo-

nents  $F_{ij}$  of  $\mathbf{F}(\mathbf{r}, 0)$  given by

$$F_{11}(\mathbf{r}) = \frac{1}{2} - \frac{2}{3} \cos \frac{3q_m x}{2} \cos \frac{\sqrt{3}q_m y}{2} + \frac{1}{6} \cos \sqrt{3}q_m y, \quad (33a)$$

$$F_{22}(\mathbf{r}) = \frac{1}{2} (1 - \cos \sqrt{3}q_m y), \quad (33b)$$

$$F_{12}(\mathbf{r}) = \frac{\sqrt{3}}{3} \sin \frac{3q_m x}{2} \sin \frac{\sqrt{3}q_m y}{2}. \quad (33c)$$

In the spirit of Leggett [24], we perform a variational calculation for a phase profile  $\varphi(\mathbf{r})$  that depends separately on  $x$  or  $y$  only. We can then bound the eigenvalues of  $\mathbf{D}_s$  by looking at the largest and smallest values (as a function of  $\theta$ ) of either of the quantities

$$A^{xx}(\theta) \equiv 8bq_m^2 n \left\langle \frac{1}{\langle F_{11}(\mathbf{r}(\theta), \theta) \rangle_{\hat{\mathbf{y}}}} \right\rangle_{\hat{\mathbf{x}}}^{-1}, \quad (34a)$$

$$A^{yy}(\theta) \equiv 8bq_m^2 n \left\langle \frac{1}{\langle F_{22}(\mathbf{r}(\theta), \theta) \rangle_{\hat{\mathbf{x}}}} \right\rangle_{\hat{\mathbf{y}}}^{-1}. \quad (34b)$$

There are three directions in which each of these quantities vanish, which coincide with the angles at which one of the three ordering momenta is perpendicular to the corresponding direction. Meanwhile, the largest eigenvalue is at most  $4bq_m^2 n$ , precisely half of the longitudinal stiffness of the FF case.

Altogether, these results imply that the superfluid response of a condensate on a moat band can be very different from that of a traditional BEC. The FF phase, while spatially homogeneous like a normal zero-momentum BEC, exhibits a highly anisotropic superfluid behavior whose directional dependence is dictated by the ordering momentum of the many-body wave function. More precisely, the superfluid current is maximal along the direction specified by  $\mathbf{q}$  and vanishes in the perpendicular direction. Similarly, in the triangle phase, the superfluid flow vanishes in the three directions perpendicular to one of the ordering momenta and becomes maximal in between.

## V. GROSS-PITAEVSKII APPROACH TO PERIODIC EXCITON CONDENSATES

In Sec. III we have presented the competition between BEC and noncondensate CSL phases. In the remainder of the article we assume that the conditions are such that the BEC phases are more stable than the CSL, for instance because of the warping effects due to the discrete rotational symmetry of the underlying lattice. In order to explore the qualitative behavior of inhomogeneous and supersolid exciton BECs in a larger region of the parameter space, in this and following sections we will replace the full  $T$  matrix by a local pseudopotential that can be used as a first approximation to a more accurate full calculation along the lines of the previous sections. This greatly

simplifies the numerical treatment and allows for analytical results with more physical insight. Under these approximations, we give necessary conditions for supersolid formation, present numerical phase diagrams, and develop an analytical Landau theory that matches them accurately.

### A. Interaction conditions and pseudopotential approximation

As we explained in detail in Sec. II, the presence or absence of inhomogeneous and supersolid BEC states crucially depends on the features of the renormalized interaction or  $T$  matrix. We have seen that even a fully repulsive (but long-ranged) exciton–exciton interaction can give rise to such states when the correct  $T$  matrix is computed. However, the full self-consistent problem is numerically expensive and not particularly physically transparent. To connect with the more familiar treatment of atomic BECs, in this and the following sections we replace the full  $T$  matrix by a local function, which allows us to use a standard Gross–Pitaevskii framework. To this end we must make sure that our choice for  $T(\mathbf{r})$  is compatible with the formation of inhomogeneous BECs, which leads to the following conditions. Firstly, for any condensate to be stable, the zero-momentum component  $T_0$  must be positive. Furthermore, it is easy to show that an inhomogeneous BEC can only arise in the presence of a negative minimum in Fourier space [49, 50]. In summary, we need  $T_0 > 0$  and  $T_k < 0$  for some nonzero  $k$ .

A negative Fourier component in the  $T$  matrix can appear when the bare interaction potential supports the formation of bound states, similar to the situation in Ref. [64], where oscillations in the  $T$  matrix are observed at energies close to the formation of a bound (or quasi-bound) state. Furthermore, the excitonic  $T$ -matrix approach of Refs. [27, 28] also introduces an oscillatory behavior to the effective interaction by cutting off the bare potential at distances smaller than some  $R_c$  below which the pair-correlation function vanishes at low densities. In view of these observations and for simplicity, in the remainder of this paper we will replace the full two-exciton  $T$  matrix by a soft-core pseudopotential of the form

$$T^{\text{sc}}(r) = \begin{cases} U_{\text{sc}} & \text{if } r \leq r_{\text{sc}}, \\ 0 & \text{if } r > r_{\text{sc}}. \end{cases} \quad (35)$$

Here,  $U_{\text{sc}}$  is the strength of the soft-core repulsion and  $r_{\text{sc}}$  the effective interaction range. The associate  $T$ -matrix kernels in 1D and 2D are given by

$$t_{\tilde{q}}^{\text{sc}} = \begin{cases} \sin \tilde{q}/\tilde{q} & \text{in 1D,} \\ J_1(\tilde{q})/\tilde{q} & \text{in 2D.} \end{cases} \quad (36a)$$

$$(36b)$$

which are oscillating and feature a series of decaying negative minima away from the origin. As can be seen from Eq. (45) below, making this pseudopotential approximation has the added benefit of reducing the problem to only two dimensionless parameters, namely  $\lambda$  and the effective interaction strength  $\Lambda \equiv 2\rho^2\gamma$ .

### B. Gross–Pitaevskii equation and periodic BECs

Having introduced a local  $T$  matrix  $T(\mathbf{r})$  we can now derive a Gross–Pitaevskii framework for the exploration of periodic BEC states on a moat band. As in Sec. III A, at the mean-field level we assume that all  $N$  excitons have condensed and the many-body wave function of the system is written as a product of identical single-particle wave functions as  $\Psi(\{\mathbf{r}_i\}) = \prod_{i=1}^N \psi(\mathbf{r}_i)$ . For convenience we define the so-called condensate wave function  $\phi(\mathbf{r}) = \sqrt{N}\psi(\mathbf{r})$ , which satisfies the normalization condition

$$\int d^2r |\phi(\mathbf{r})|^2 = N. \quad (37)$$

The mean-field free energy of a spinless Bose gas with a moat dispersion interacting via an effective local  $T$  matrix  $T(\mathbf{r})$  then reads

$$\mathcal{F} = \int d^2r \phi^*(\mathbf{r}) \left( \frac{a^2}{4b} - a\mathbf{p}^2 + b\mathbf{p}^4 \right) \phi(\mathbf{r}) + \frac{1}{2} \int d^2r d^2r' \phi^*(\mathbf{r}) \phi^*(\mathbf{r}') T(\mathbf{r} - \mathbf{r}') \phi(\mathbf{r}') \phi(\mathbf{r}). \quad (38)$$

Minimizing Eq. (38) and introducing a Lagrange multiplier  $\mu N$  to impose the particle number constraint yields the Gross–Pitaevskii equation (GPE)

$$\left( \frac{a^2}{4b} - a\mathbf{p}^2 + b\mathbf{p}^4 + T_{\phi}^{\text{eff}}(\mathbf{r}) - \mu \right) \phi(\mathbf{r}) = 0, \quad (39)$$

where we have defined

$$T_{\phi}^{\text{eff}}(\mathbf{r}) \equiv \int d^2r' T(\mathbf{r} - \mathbf{r}') |\phi(\mathbf{r}')|^2. \quad (40)$$

We are interested in lattice solutions for the condensate wave function, i.e., solutions where the density  $n(\mathbf{r}) = |\phi(\mathbf{r})|^2$  displays a periodic pattern. It is straightforward to show that a periodic  $|\phi(\mathbf{r})|^2$  leads to a periodic effective potential  $T_{\phi}^{\text{eff}}$ , as long as the integral kernel depends on the difference of coordinates only. Thus, the GPE of Eq. (39) takes the form of a Schrödinger equation with a periodic potential. The solution is therefore given by a Bloch wave function which we write as

$$\phi(\mathbf{r}) = \sqrt{n} e^{i\mathbf{g}\cdot\mathbf{r}} u_{\mathbf{g}}(\mathbf{r}), \quad (41)$$

where the factor of  $\sqrt{n}$  has been explicitly factored out for convenience. The Bloch factor  $u_{\mathbf{g}}(\mathbf{r})$  is a function with the same periodicity as the emerging density profile, and  $\mathbf{g}$  is a crystal momentum lying in the first Brillouin zone of the associated reciprocal space. The periodicity of  $u_{\mathbf{g}}(\mathbf{r})$  allows us to expand it in terms of reciprocal lattice vectors  $\mathbf{G}$  via

$$u_{\mathbf{g}}(\mathbf{r}) = \sum_{\mathbf{G}} u_{\mathbf{g}\mathbf{G}} e^{i\mathbf{G}\cdot\mathbf{r}}, \quad (42)$$

With  $\phi(\mathbf{r})$  written in this way, the normalization condition of Eq. (37) becomes

$$\sum_{\mathbf{G}} |u_{\mathbf{g}\mathbf{G}}|^2 = 1. \quad (43)$$

If there are  $d'$  directions in which translational symmetry is broken, the reciprocal space will be spanned by  $d'$  basis vectors. Our task will be to find the crystal momentum  $\mathbf{g}$ , the reciprocal lattice basis vectors  $\mathbf{G}_i$ , and the coefficients  $u_{\mathbf{q}\mathbf{G}}$  which minimize the free energy. In momentum space, the GPE is an equation for the expansion coefficients  $u_{\mathbf{g}\mathbf{G}}$  and takes the form

$$\varepsilon_{\mathbf{g}+\mathbf{G}} u_{\mathbf{g}\mathbf{G}} + n \sum_{\mathbf{G}'\mathbf{G}''} T_{\mathbf{G}''-\mathbf{G}'} u_{\mathbf{g}\mathbf{G}'}^* u_{\mathbf{g}\mathbf{G}''} u_{\mathbf{g},\mathbf{G}+\mathbf{G}'-\mathbf{G}''} = \mu u_{\mathbf{g}\mathbf{G}}, \quad (44)$$

where  $\varepsilon_{\mathbf{k}} = a^2/4b - ak^2 + bk^4$  is the moat dispersion. In the dimensionless units of Sec. II C, the GPE reads

$$\tilde{\varepsilon}_{\tilde{\mathbf{g}}+\tilde{\mathbf{G}}} u_{\tilde{\mathbf{g}}\tilde{\mathbf{G}}} + \Lambda \sum_{\tilde{\mathbf{G}}'\tilde{\mathbf{G}}''} t_{\tilde{\mathbf{G}}''-\tilde{\mathbf{G}}'} u_{\tilde{\mathbf{g}}\tilde{\mathbf{G}}'}^* u_{\tilde{\mathbf{g}}\tilde{\mathbf{G}}''} u_{\tilde{\mathbf{g}},\tilde{\mathbf{G}}+\tilde{\mathbf{G}}'-\tilde{\mathbf{G}}''} = \tilde{\mu} u_{\tilde{\mathbf{g}}\tilde{\mathbf{G}}}, \quad (45)$$

where  $\Lambda \equiv 2\rho^2\gamma$ . Note that 1D, which we will also consider for intuition, the parameter  $\rho$  is defined as  $\rho = \sqrt{n_{1D}r_0}$ , with  $n_{1D}$  the exciton number per unit *length*.

## VI. ONE-DIMENSIONAL LATTICES

In this section we present the phase diagram of moat-band excitons with a soft-core pseudopotential in 1D, a qualitative explanation of the underlying physics, as well as an effective Landau theory validating the numerical calculations.

### A. Numerical results

We have numerically solved Eq. (45) as a function of  $\lambda$  and  $\Lambda$  in 1D, and the resulting phase diagram is plotted in Figure 5. In the 1D case, there are three possible phases. The dark-green region corresponds to a condensate with a constant order parameter, and is simply dubbed the BEC phase for simplicity. By contrast, the light-green region corresponds to the homogeneous FF phase, while the yellow region is the LO or stripe phase, featuring an inhomogeneous periodic density profile.

We can qualitatively understand the phase diagram as follows. For positive  $\lambda$  the dispersion is convex and its minimum lies at zero momentum. For small values of  $\Lambda$ , i.e., low densities and weak interactions, the bosons will tend to occupy this single momentum state and the resulting phase will be the homogeneous BEC. However, as  $\Lambda$  increases, the situation can change in the presence of a negative minimum of the interaction potential in Fourier space. For large enough  $\Lambda$  the latter can favor the occupation of two opposite nonzero momentum states  $\pm\tilde{\mathbf{g}}$ , as the resulting increase in kinetic energy can eventually be fully compensated by the attractive coupling induced by a momentum transfer of  $2\tilde{\mathbf{g}}$ . This marks the onset of the LO phase at positive  $\lambda$ . The transition from the BEC to the LO phase is discontinuous, which can be understood from the fact that the ordering momentum  $\tilde{\mathbf{g}}$  jumps from zero

in the BEC phase to a nonzero value such that  $t_{2\tilde{\mathbf{g}}} < 0$ . When  $\lambda$  is small and negative and  $\Lambda$  is also small, all particles again sit at the state of lowest kinetic energy, which is now spontaneously chosen between the two minima which constitute the moat in the 1D case. In this situation, it is unfavorable for the excitons to occupy both minima simultaneously because this yields a positive energy shift due to the potential at momentum transfer  $2q_m$ , which is positive for a small moat momentum. Thus, in this regime we find the FF phase. The transition from the BEC to the FF phase as we tune  $\lambda$  from positive to negative is a Lifshitz transition and thus continuous, as in fact the BEC can simply be understood as an FF phase with zero momentum. For small and negative  $\lambda$ , increasing  $\Lambda$  leads to the same physics explained above, and we eventually reach a discontinuous phase transition from the FF to the LO state. As  $\lambda$  is made more negative and the moat increases in size, this transition takes place at increasingly small values of  $\Lambda$ , because the momentum transfer  $2q_m$  becomes closer to the point where the interaction kernel  $t$  changes sign. Eventually we reach a point where  $t_{2\tilde{\mathbf{q}}_m} = 0$ , which for the 1D case with  $t_{\tilde{\mathbf{k}}} = \sin \tilde{k}/\tilde{k}$  occurs at  $2\tilde{q}_m = \pi$ , or  $\lambda = -\pi^2/4 \approx -2.47$ . At this point the barrier for the creation of an inhomogeneous BEC is completely removed and any positive  $\Lambda$ , no matter how small, will stabilize the LO phase. We thus conclude that a moat dispersion can lead to a stripe phase already in the regime of low densities and weak interactions.

We also note that decreasing  $\lambda$  beyond the region shown in the phase diagram of Figure 5 eventually results in a reentrant FF phase and a subsequent alternating behavior of the FF and LO phases. This can be fully understood analytically and is explained in the following section.

In Figure 6 we have plotted the numerically obtained density profiles for several values of  $\Lambda$  at fixed  $\lambda$ , and vice-versa. As  $\Lambda$  increases, the high-density regions start to become more peaked and the profile between the peaks starts to flatten out. This is because for large  $\Lambda$  the interaction dominates and the condensate can lower its energy by forming regions of vanishing density and localizing the latter in increasingly small patches. Meanwhile, as  $\lambda$  decreases, the periodicity of the density profile decreases as well. This can be easily understood for small  $\Lambda$ , as in this case the ordering momentum will be close to the moat momentum  $q_m$ , which increases with decreasing  $\lambda$  and tends to realize smaller lattices.

### B. Analytical Landau theory

All phase transitions in 1D can be further understood analytically by writing down an effective Landau theory for the condensate wave function. Inspired by the numerical results, we write it in terms of only two nonzero coefficients as

$$\phi(x) = \sqrt{n} (u_1 e^{ig_1 x} + u_2 e^{ig_2 x}), \quad (46)$$

where we assume that  $g_1 \neq g_2$ . Note that we have absorbed the momentum  $g$  of the expansion in Eq. (41) inside the reciprocal lattice vectors  $G$ . The (dimensionless) free energy per particle

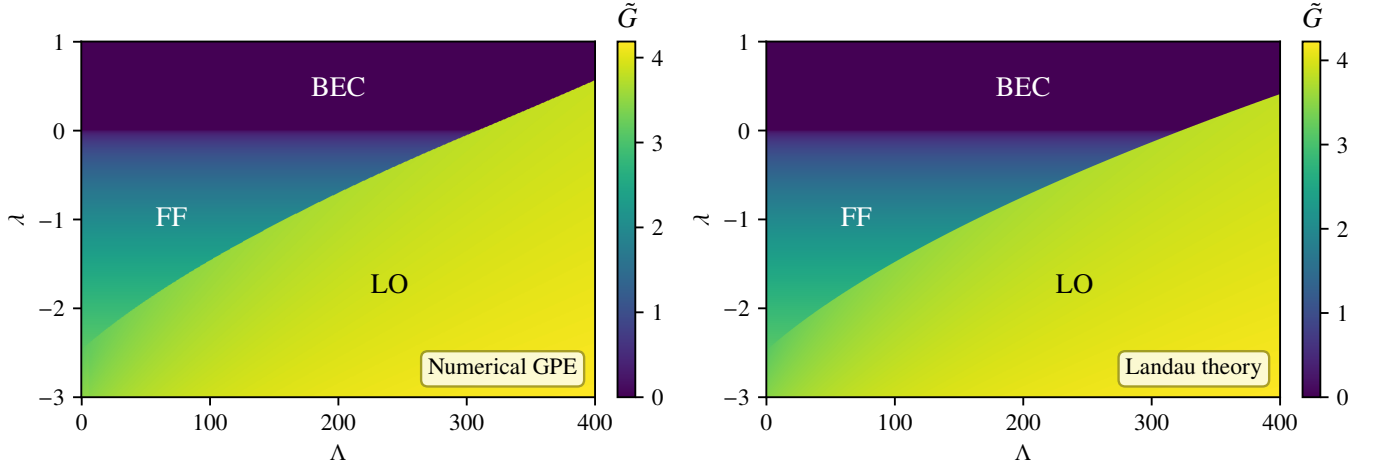


FIG. 5. Phase diagram of 1D moat-band excitons with a soft-core interaction  $T^{\text{sc}}(x) = U_{\text{sc}}\Theta(1 - |x|/r_{\text{sc}})$ . The parameter  $\lambda$  is related to the moat size (when  $\lambda < 0$ ) and  $\Lambda$  is an effective interaction strength. The left plot shows the result of the full numerical GPE calculation, while the right plot shows the result of the analytical Landau theory. The color coding represents the length of the momentum vector  $G$  characterizing each phase, made dimensionless via  $\tilde{G} = Gr_{\text{sc}}$ . The BEC has a constant wave function,  $\phi_{\text{BEC}}(x) = \sqrt{n}$  with  $n$  the exciton number density, while the FF phase has  $\phi_{\text{FF}}(x) = \sqrt{n}e^{i(G/2)x}$  with  $G = 2q_m$ . These two phases give a homogeneous density profile. In the LO phase, the order parameter near the transition behaves as  $\phi_{\text{LO}}(x) \propto \cos(Gx/2)$ , leading to a lattice constant  $2\pi/G$  for the density profile  $|\phi(x)|^2$ . The transition between the BEC and FF phases at  $\lambda = 0$  is continuous, while that between the homogeneous phases and the LO phase is discontinuous. For a large moat, i.e., negative enough  $\lambda$ , an inhomogeneous BEC exists even in the limit of weak interactions and low exciton density. The simple Landau theory is in excellent quantitative agreement with the full numerical result in the region of this plot. Deviations start to occur at large  $\Lambda$ , where the density peaks localize and the order parameter cannot be written as a simple cosine.

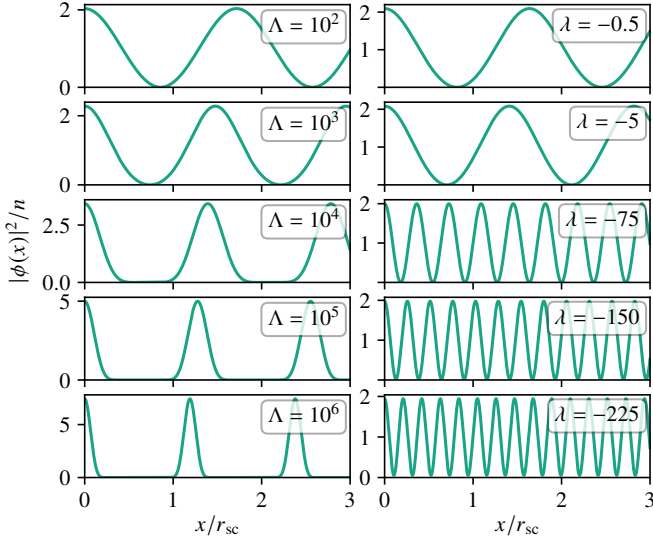


FIG. 6. Density profile of the 1D LO phase for different values of the parameters. The left column corresponds to a fixed value of  $\lambda = -2$  while the right column corresponds to  $\Lambda = 300$ . The lattice constant  $a$  is related to the 1D ordering vector  $G$  via  $a = 2\pi/G$ . For modest values of  $\Lambda$  the profile is very close to a perfect cosine and the Landau theory developed in Sec. VIB gives quantitatively accurate results. For very large values of  $\Lambda$  the peaks localize and the Landau theory breaks down as we go deep inside the LO phase.

$\tilde{f} \equiv (F/N)/(b/r_{\text{sc}}^4)$  with this ansatz reads

$$\begin{aligned} \tilde{f} = & |u_1|^2 \tilde{\varepsilon}_{\tilde{g}_1} + |u_2|^2 \tilde{\varepsilon}_{\tilde{g}_2} \\ & + \frac{\Lambda}{2} t_0 (|u_1|^2 + |u_2|^2)^2 + \Lambda t_{\tilde{g}_1 - \tilde{g}_2} |u_1|^2 |u_2|^2, \end{aligned} \quad (47)$$

which we must minimize with respect to  $u_1$ ,  $u_2$ ,  $\tilde{g}_1$ , and  $\tilde{g}_2$  under the constraint  $|u_1|^2 + |u_2|^2 = 1$ . The latter is introduced via a Lagrange multiplier which is simply the chemical potential,  $\tilde{f} \rightarrow \tilde{f} - \tilde{\mu}(|u_1|^2 + |u_2|^2 - 1)$ . It is clear from Eq. (47) that a relative phase between  $u_1$  and  $u_2$  does not influence the free energy, which can be seen from the fact that such a shift simply corresponds to a horizontal displacement of the density profile generated by  $\phi(x)$ . Thus, we assume without loss of generality that both  $u_1$  and  $u_2$  are real and positive. Note that this will not always be the case in two dimensions.

Firstly, we find trivial solutions which have  $u_1 = 1$  and  $u_2 = 0$ , or  $u_1 = 0$  and  $u_2 = 1$ . For these, the momentum associated with the nonzero component is zero when  $\lambda > 0$  and  $\pm \tilde{q}_m$  when  $\lambda < 0$ , which correspond to the BEC and FF phases, respectively. The chemical potential is given by  $\tilde{\mu} = \lambda^2 + \Lambda t_0$  for  $\lambda > 0$  and  $\tilde{\mu} = \Lambda t_0$  for  $\lambda < 0$ . Whether or not these homogeneous phases correspond to the ground state of the system for positive or negative  $\lambda$  will depend on the specific value of  $\Lambda$ , which is present in the two terms on the second line of Eq. (47). The  $t_0$  term has no effect due to the normalization constraint, which effectively results in an overall shift irrespective of  $u_1$  and  $u_2$ . However, from the last term of Eq. (47) we see that  $\Lambda$  couples to the potential at the momentum transfer  $\tilde{g}_1 - \tilde{g}_2$ . Thus, it is clear that a negative Fourier component at nonzero momentum can lower

the overall energy and thus give rise to periodic solutions.

Secondly, we find nontrivial solutions where both coefficients are nonzero and satisfy  $u_1 = u_2 = 1/\sqrt{2}$ . These have  $\tilde{g}_1 = -\tilde{g}_2 \equiv \tilde{G}/2$  and  $\tilde{\mu} = \tilde{\varepsilon}_{\tilde{G}/2} + \Lambda(t_0 + \frac{1}{2}t'_{\tilde{G}})$  [65]. Without loss of generality we take  $\tilde{G} > 0$ . Unlike for the trivial solutions with one of the coefficients equal to zero, the value of  $\tilde{g}$  now depends on the details of the interaction kernel  $t$  and is found by solving the transcendental equation

$$\tilde{G}(\tilde{G}^2 + 4\lambda) + \Lambda t'_{\tilde{G}} = 0, \quad (48)$$

where  $t'$  stands for the derivative of  $t$  with respect to its argument. In the case of a soft-core potential in 1D, we have  $t'_{\tilde{G}} = (\tilde{G} \cos \tilde{G} - \sin \tilde{G})/\tilde{G}^2$ . The values of  $\lambda$  and  $\Lambda$  determine whether the transcendental equation (48) has a nontrivial solution for  $\tilde{G}$ . Plotting the function for  $\lambda > 0$ , i.e., in the absence of a moat, reveals that nontrivial solutions for  $\tilde{G}$  exist only when  $\Lambda$  exceeds some ( $\lambda$ -dependent) critical value. Therefore, periodic solutions in the absence of a moat require relatively high densities or strong interactions. Meanwhile, for  $\lambda < 0$  there always exists a nontrivial solution for  $\tilde{G}$ , even in the limit of  $\Lambda \rightarrow 0$ , where evidently  $\tilde{G} = 2\tilde{q}_m$ . This signals that periodic solutions exist no matter the density or interaction strength. For small  $\Lambda$ , we can find the momentum of the density lattice to linear order as

$$\tilde{G} = 2\tilde{q}_m + \frac{\Lambda}{2(2\tilde{q}_m)^4}(\sin 2\tilde{q}_m - 2\tilde{q}_m \cos 2\tilde{q}_m) + \mathcal{O}(\Lambda^2). \quad (49)$$

Thus, in this particular model, turning on the interactions leads to an initial growing or shrinking of the lattice constant of the BEC, depending on the size of the moat.

By comparing the free energy of the solutions we have discussed we obtain the phase diagram of the Landau theory, which is plotted in Figure 5. We see that the agreement with the full numerical calculation is excellent and only starts deviating slightly for large  $\Lambda$ , the reason being that in this regime the peaks of  $\phi(x)$  start to localize and we would need to include more coefficients into the expansion of Eq. (46).

We can use the analytical Landau theory to extend the phase diagram outside of the region for which the phase diagram was obtained numerically. In Fig. 7 we plot the phase diagram for large negative values of  $\lambda$ . While the latter are most certainly unrealistic, the extended phase diagram further helps in understanding the underlying physics. As  $\lambda$  decreases, the LO phase and the FF phase begin to alternate, which is a consequence of the oscillating nature of the soft-core potential in momentum space. As we decrease  $\lambda$  and thus the moat size, the potential  $t$  will vanish at specific values of the moat momentum transfer  $2q_m$ . This leads to a change of sign in the interaction energy associated with coupling both sides of the moat and thus results in a back-and-forth behavior between the FF and LO phases. In 1D and for a soft-core interaction, these transitions take place at  $\lambda = -l^2\pi^2/4$ , where  $l$  is a nonzero integer. Furthermore, every time we reenter the LO phase the associated reciprocal lattice vector becomes larger and therefore the periodicity of the density pattern is smaller. If the Fourier transform of the

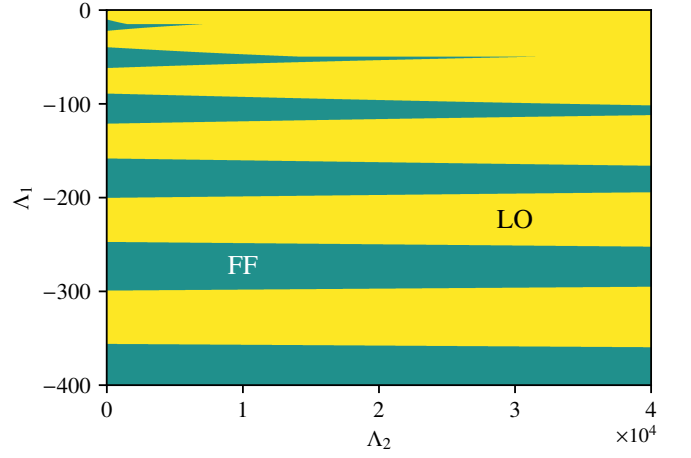


FIG. 7. Extended phase diagram for one-dimensional moat-band excitons with a soft-core potential resulting from the analytical Landau theory developed in the main text. For  $\lambda < 0$ , the oscillations of the interaction potential in momentum space lead to a reentrant behavior between the FF and LO phases. For small  $\Lambda$  these transitions take place at  $\lambda = -l^2\pi^2/4$  with integer  $l > 0$ , which are the points where the moat momentum transfer  $2q_m$  causes the potential kernel to change sign. Note that here the color coding only serves to distinguish the phases and does not represent the length of the characteristic momentum.

interaction potential were only to change sign once and stay negative above some value of the momentum, then there would be no reentrant behavior and the LO phase would be present for all values below the critical  $\lambda$ .

It is worth mentioning that we have also considered a Landau theory for three order parameters,  $\phi(x) = \sqrt{n}(u_0 + u_+e^{igx} + u_-e^{-igx})$ , which would describe a hybrid zero-momentum–LO phase similar to that of Eq. (16). The free energy in this case reads

$$\begin{aligned} \tilde{f} = & |u_0|^2 \tilde{\varepsilon}_0 + (|u_+|^2 + |u_-|^2) \tilde{\varepsilon}_{\tilde{g}} + \Lambda t_{\tilde{g}} |u_0^* u_+ + u_-^* u_0|^2 \\ & + \frac{\Lambda}{2} t_0 (|u_0|^2 + |u_+|^2 + |u_-|^2)^2 + \Lambda t_{2\tilde{g}} |u_+|^2 |u_-|^2. \end{aligned} \quad (50)$$

However, we have found that the energy of such a hybrid phase is always higher than that of one of the pure phases, and thus it does not appear in the considered region of the parameter space, in accordance with the full numerical calculation. We note that this is an artifact of the quartic dispersion that we are using. In 1D, as pointed out in Ref. [49], a quadratic dispersion with a long-range interaction identical to the one considered here yields a mixed phase in a restricted region of the parameter space. We have checked that this phase disappears upon the use of a quartic dispersion, so there is no contradiction.

## VII. TWO-DIMENSIONAL LATTICES

In this section we provide the phase diagram of two-dimensional moat-band excitons. Having built intuition via the 1D case, it is relatively straightforward to understand the physics in a 2D scenario. Here the analysis is complicated

slightly by the fact that there are several distinct candidate lattice structures. These must in principle be compatible with the discrete rotational symmetry of the underlying lattice in order to accommodate for the warping effects described in Sec. III D. In our calculations, where for simplicity we use a perfect moat, we have considered a broken translational symmetry in one direction and broken translational symmetry in two directions for a triangular lattice and a square lattice. While the former (which leads to a stripe phase) is compatible with any lattice structure, the latter must be chosen depending on the discrete rotational symmetry of the lattice. Thus, a  $C_3$ - or  $C_6$ -invariant system will be compatible with a triangular phase, while a  $C_4$ -invariant system will be compatible with a square phase.

### A. Numerical results

We numerically obtain the phase diagram involving the three aforementioned lattices by solving the momentum-space GPE with such an ansatz and minimizing the energy with respect to the length of the reciprocal lattice vector, and then comparing the energies obtained for the different structures. The result is plotted in Fig. 8, where we focus on the  $\lambda < 0$  case as for positive  $\lambda$  the situation is similar to that in the 1D case. As in 1D case, for small  $\lambda$  and  $\Lambda$  we obtain a homogeneous FF phase which is eventually replaced by a stripe or LO phase when either  $\Lambda$  becomes larger or  $\lambda$  becomes more negative. Furthermore, for even larger  $\Lambda$  or larger moats we obtain a triangular phase where the translational symmetry is broken in both directions. Even deeper in the phase diagram we have obtained a square lattice, although this region is not shown in the plot. These transitions are all of first order. We also plot two examples of the density profile in the triangular phase for a fixed value of  $\lambda$ . A similar behavior as for the 1D case can be seen when increasing  $\Lambda$ , by which the peaks tend to localize and the regions between the peaks flatten out.

### B. Analytical Landau theories

In this section we consider Landau theories for the transitions between the 2D periodic BECs at small  $\Lambda$ , which if desired can be extended to all  $\Lambda$  via the methods introduced in Sec. VI B. The transition between the FF phase and the LO can be understood analytically via the same Landau theory that we used in 1D by simply adding a second component to the momentum and assuming that there is no symmetry breaking along that direction. The only difference is that the soft-core interaction kernel is now  $t_{\tilde{G}} = J_1(\tilde{G})/\tilde{G}$ , whose derivative entering Eq. (48) reads  $t'_{\tilde{G}} = -J_2(\tilde{G})/\tilde{G}$ . This leads to the same qualitative behavior explained in the previous section and only changes the value of  $\lambda$  at which the transition occurs. The latter can be determined by finding the point at which  $t_{2\tilde{q}_m}$  changes sign and yields  $\lambda \approx -3.67$ , somewhat higher than for the 1D case where  $\lambda \approx -2.47$ . Once again the results are in excellent agreement with the numerics and for this reason we do not display them further.

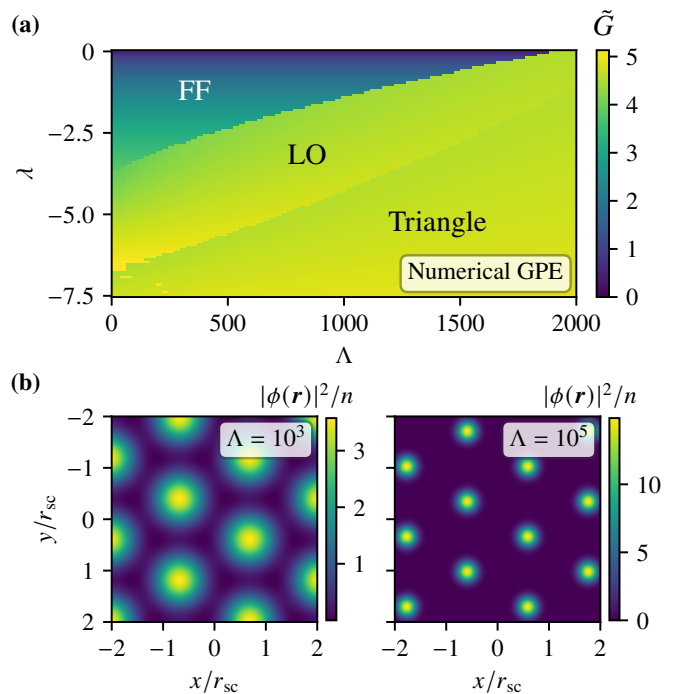


FIG. 8. (a) Phase diagram of 2D moat-band excitons with a soft-core interaction  $T^{sc}(r) = U_{sc}\Theta(1 - r/r_{sc})$ . The parameters  $\lambda$  and  $\Lambda$  have the same interpretation as in the 1D case and we do not show the constant BEC present at  $\lambda > 0$ . The FF and LO phases have the same wave function as in the 1D case, while the triangle phase has three coefficients located at the vertices of an equilateral triangle. The artifacts in the bottom left corner are due to numerical instabilities at small  $\Lambda$ . (b) Density profiles of the triangle phase for  $\lambda = -5$  and two values of the interaction parameter  $\Lambda$ .

We can also obtain the critical value of  $\lambda$  at which the transition from the LO to the triangle phase occurs at small  $\Lambda$ . In this case we must compare the interaction energy in each of the two phases as a function of the moat size. In the LO phase, the interaction energy (without the zero point common to all phases) is  $\tilde{f}_{\text{int}}^{(2)} = \Lambda t_{2\tilde{q}_m} |u_+|^2 |u_-|^2$ , with  $|u_+| = |u_-| = 1/\sqrt{2}$  the coefficients of  $\phi(\mathbf{r})$  at opposite sides of the moat of radius  $q_m$ . In the triangle phase, it is given by  $\tilde{f}_{\text{int}}^{(3)} = \Lambda t_{\sqrt{3}\tilde{q}_m} (|u_1|^2 |u_2|^2 + |u_2|^2 |u_3|^2 + |u_3|^2 |u_1|^2)$ , with  $|u_1| = |u_2| = |u_3| = 1/\sqrt{3}$  the coefficients of three points on the moat forming an equilateral triangle with the length of each side equal to  $\sqrt{3}q_m$ . Comparing the two, we conclude that the moat momentum at which the LO-to-triangle transition occurs is found by solving the transcendental equation

$$t_{2\tilde{q}_m} - \frac{4}{3} t_{\sqrt{3}\tilde{q}_m} = 0. \quad (51)$$

For the 2D soft-core interaction this leads to  $\Lambda_1 \approx -6.65$ , in perfect agreement with the numerical calculation of Fig. 8.

While we have not extended the phase diagram to very negative values of  $\lambda$ , we can use the procedure above to infer the presence of other lattice structures deeper in the phase diagram. For instance, let us consider a square phase with

coefficients  $u_1, u_2, u_3, u_4$  corresponding to the points  $(q_m, 0)$ ,  $(0, q_m)$ ,  $(-q_m, 0)$ , and  $(0, -q_m)$  in momentum space, respectively, which form a square with diagonal  $2q_m$ . The interaction energy reads

$$\begin{aligned} \tilde{f}_{\text{int}}^{(4)} = & \Lambda t_{2\tilde{q}_m} (|u_1|^2 |u_3|^2 + |u_2|^2 |u_4|^2) \\ & + \Lambda t_{\sqrt{2}\tilde{q}_m} (|u_1|^2 |u_2|^2 + |u_2|^2 |u_3|^2 + |u_3|^2 |u_4|^2 \\ & + |u_4|^2 |u_1|^2 + 2u_1^* u_3^* u_2 u_4 + 2u_2^* u_4^* u_1 u_3). \end{aligned} \quad (52)$$

which can be found geometrically by considering all scatterings with nonzero momentum transfer and equal total ingoing and outgoing momenta, and counting the multiplicities of these processes. Particular attention must be paid to the last two terms, which depend on the relative phases of the four coefficients. While we expect that  $|u_1| = |u_2| = |u_3| = |u_4| = 1/2$ , depending on the sign of  $t_{\sqrt{2}\tilde{q}_m}$  we will have to choose the sign of  $u_1^* u_3^* u_2 u_4$  to be  $+1$  or  $-1$  in order to lower the total energy. Taking this into account, we find that at small  $\Lambda_2$  there will be a transition from the triangle phase to the square phase at the moat momentum that solves the equation

$$t_{2\tilde{q}_m} + 2(t_{\sqrt{2}\tilde{q}_m} - |t_{\sqrt{2}\tilde{q}_m}|) - \frac{8}{3} t_{\sqrt{3}\tilde{q}_m} = 0. \quad (53)$$

This gives  $\lambda \approx -8.75$  for the 2D soft-core potential.

The derived triangle-to-square transition is theoretically only valid in the limit of a perfectly degenerate moat, i.e., in the absence of warping, so that it is simultaneously compatible with both a triangle phase and a square phase. However, since  $\lambda = -(q_m r_{\text{sc}})^2$ , we need relatively large moats for a reasonable interaction ranges of a few nm. If the moat is perfectly degenerate this will almost certainly lead to the CSL state at dilute enough densities, while if warping is present one of the two phases will not be compatible with the lattice structure. In other words, this triangle-to-square transition seems unlikely in real physical systems. In a  $C_3$ - or  $C_6$ -symmetric system we expect a hexagonal phase after the triangular one, while in a  $C_4$ -symmetric system it is reasonable to expect the LO to directly give rise to a square phase.

Let us now consider these more realistic scenarios by focusing on a  $C_3$ -symmetric system with six minima around the moat as in Fig. 4. We assume that  $\Lambda$  is small enough so that the many-body wave function is indeed locked into the minima of the dispersion, and consider the small interaction energy as a perturbation lifting the degeneracy of the different possible phases. There are three possibilities for a stripe phase, which arise from the three inequivalent ways in which we can distribute two nonzero coefficients among the six minima of the moat. We can summarize this by writing the stripe interaction energy as

$$\tilde{f}_{\text{int}}^{(2)} = \frac{1}{\Lambda} \min(t_{\tilde{q}_m}, t_{\sqrt{3}\tilde{q}_m}, t_{2\tilde{q}_m}). \quad (54)$$

Assuming equal weights for the coefficients, there are also

three possible inequivalent triangle phases, so that

$$\frac{\tilde{f}_{\text{int}}^{(3)}}{\Lambda} = \frac{1}{9} \min(t_{\tilde{q}_m} + t_{\sqrt{3}\tilde{q}_m} + t_{2\tilde{q}_m}, 2t_{\tilde{q}_m} + t_{\sqrt{3}\tilde{q}_m}, 3t_{\sqrt{3}\tilde{q}_m}), \quad (55)$$

where the last possibility corresponds to the equilateral case. Finally, the interaction energy of the  $C_3$ -compatible hexagonal phase reads

$$\frac{\tilde{f}_{\text{int}}^{(6)}}{\Lambda} = \frac{t_{2\tilde{q}_m}}{12} + \frac{5}{24} (t_{\tilde{q}_m} + t_{\sqrt{3}\tilde{q}_m}) - \frac{1}{8} |t_{\tilde{q}_m} + t_{\sqrt{3}\tilde{q}_m}|, \quad (56)$$

where again we have assumed equal  $|u_i|$ . Note that for the hexagonal phases we have chosen the phases of the coefficients in such a way that they will always minimize the energy depending on the sign of the interaction at the accompanying momentum transfer [66]. The assumption of equal  $|u_i|$  is justified in view of the observation that, in a situation where having unequal coefficients lowers the energy, there will be a stripe phase that is even more stable and which we are already considering. This relies on the fact that our soft-core interaction in momentum space has one single dominant minimum. In situations with several competing minima the situation is more complicated, and for a perfectly degenerate moat could lead to anisotropic phases or even quasicrystals due to the presence of two or more competing length scales in the interaction potential [67–70]. Such an interaction seems rather unnatural for an excitonic system and we do not explore these possibilities any further in this article.

In Fig. 9 we have plotted the interaction energies of Eqs. (54)–(56). As long as  $\tilde{f}_{\text{int}} < 0$ , the lowest curve will correspond to the most stable phase. In practice we find that when the triangular phase is stabilized this is always in the form of the equilateral phase, which relates to our comment about the potential possessing a single absolute minimum in Fourier space. It is worth mentioning that we have also considered a rectangular phase on four minima of the dispersion, but its energy is always higher and we do not show the corresponding curve. As explained earlier, we indeed find that there is a transition from the triangle phase to the hexagonal phase, and we can solve for the associated critical  $\lambda$  by solving the transcendental equation

$$t_{\sqrt{3}\tilde{q}_m} + |t_{\tilde{q}_m} + t_{\sqrt{3}\tilde{q}_m}| - \frac{2}{3} t_{2\tilde{q}_m} - \frac{5}{3} t_{\tilde{q}_m} = 0. \quad (57)$$

This leads to  $\lambda \approx -15.16$  and corresponds to  $\tilde{q}_m \approx 3.89$ , which is clearly seen in the inset of Fig. 9. Similarly we can also find the LO-to-square transition expected in a  $C_4$ -symmetric system by solving

$$t_{2\tilde{q}_m} + 2|t_{\sqrt{2}\tilde{q}_m}| - 2t_{\sqrt{2}\tilde{q}_m} = 0, \quad (58)$$

which yields  $\lambda \approx -7.92$ .

### C. Estimates for real systems

Let us finally give a rough estimate of the parameter  $\lambda$  corresponding to the Bernevig–Hughes–Zhang model for bismuth

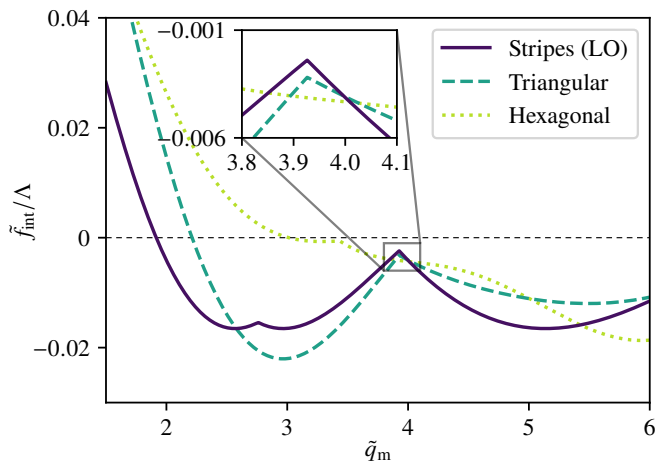


FIG. 9. Soft-core interaction energies in 2D for different  $C_3$ -compatible periodic lattices for small  $\Lambda$  as a function of the moat momentum, corresponding to Eqs. (54)–(56) of the main text. The different phases correspond to a momentum-space order parameter with  $n$  coefficients of equal magnitude distributed on the minima of the moat, with  $n = 2, 3, 6$ . For  $\tilde{q}_m < 1.92$ , which corresponds to  $\lambda \approx -3.67$ , the most stable phase is the homogeneous FF phase with vanishing energy. Above this value, the state of lowest energy changes as a function of  $\tilde{q}_m$ , giving rise to inhomogeneous and supersolid phases with different degrees of discrete rotational symmetry. The kinks in the square and hexagonal interaction energy curves correspond to changes in the optimal choice of phases for the coefficients as well as different combinations of the populated minima, as explained in the main text. In this range of  $\tilde{q}_m$ , a stable triangular phase is always found to be equilateral. The inset shows a small region where a hexagonal phase is stabilized.

selenide explored in Ref. [21], which would be subject to hexagonal warping due to the  $C_3$  symmetry of the lattice. We obtained a moat momentum of the order of  $0.5\text{--}1\text{ nm}^{-1}$ , with an energy barrier of a few tens of meV. While the exciton–exciton interaction is expected to be complicated, we match it to the soft-core potential by using an effective range  $r_{sc} \sim 1\text{--}10\text{ nm}$ , which is of the order of the exciton diameter for the lowest-lying modes. This gives  $\lambda = -(q_m r_{sc})^2$  between  $-0.25$  and  $-100$  for the most conservative and the most optimistic cases, respectively. The magnitude of  $\Lambda$  is more difficult to estimate due to the uncertainty regarding the effective exciton–exciton interaction strength; nevertheless, our estimate of  $\lambda$  shows that a real exciton system has the chance of sitting in the inhomogeneous (and possibly even supersolid) region of the phase diagram in Fig. 8, even in the case of low densities and weak interactions.

## VIII. CONCLUSION AND OUTLOOK

In this article we have explored the possible phases of a dilute system of excitons with moat bands, where the low-energy degrees of freedom lie on a circle around some high-symmetry point in the Brillouin zone. In the assumption of a perfectly degenerate moat, we have reviewed how the ex-

citons may undergo statistical transmutation to fermions with a flux attachment. At low densities they can then realize a chiral spin liquid phase in which the emergent fermions sit in a fully filled Landau level generated by the resulting effective magnetic field, while we have shown that long-range interactions eventually drive a transition to a Bose–Einstein condensate phase at higher densities. We then argued that the warping of the band structure due to the underlying lattice of real systems will tend to break the perfect degeneracy of the moat. As a result, the latter acquires a finite number of minima separated by an energy barrier which at low temperatures is high enough to lock the excitons to these points of lowest energy. Consequently, BEC phases become the most likely outcome in the event of excitonic condensation. We have shown that the  $T$ -matrix renormalization of the bare exciton–exciton interaction can lead to the emergence of periodic and supersolid exciton BECs and presented corresponding self-consistent calculations. Furthermore, the superfluid response of these supersolids is unusual due to the presence of the moat, leading to a strong directional anisotropy depending on the spatial symmetry of the periodic density pattern. We have further explored the phase diagram of excitonic condensates via a soft-core pseudopotential approximation. While in the case of a normal parabolic dispersion these periodic states can only exist in the regime of high densities and strong interactions, we have shown that a moat band can help stabilize them even in the regime of low densities and weak interaction strengths. Finally, we have justified that the supersolid region of the phase diagram should be experimentally accessible under the right conditions.

The work presented in this article serves as a proof of concept and constitutes a minimal model for condensation of moat-band excitons. Our theory can be expanded to include various effects which may be relevant in a variety of experimental systems. One example would be to include also the spin of the excitons, which has been ignored here in the assumption that the underlying electronic system is appropriately spin-polarized. The resulting problem can be mapped to a multi-channel Gross–Pitaevskii equation, which may exhibit richer behavior than the spinless case. For instance, in the presence of two spin species with a different interspin interaction, a  $C_6$ -symmetric supersolid phase may exhibit frustration akin to that of an antiferromagnetic Heisenberg model on a triangular lattice. From a quantitative point of view, an immediate (though numerically demanding) way to improve the calculation of the excitonic phase diagram for supersolid phases would be the implementation of a self-consistent  $T$ -matrix loop in the solution of the full Gross–Pitaevskii equation. A calculation of this nature may also employ a more realistic bare exciton–exciton interaction, for instance based on a combination of the different scattering diagrams derived in Ref. [44] which incorporate the excitonic wave functions and which may be generalized to include also band-geometrical, topological, or moiré effects.

Our results and speculations on further work indicate that moat-band excitons constitute a promising platform to explore correlated bosonic phases with long-range entanglement or superfluid order even in the case of dilute systems at weak coupling. The potential presence of an excitonic moat band

can often be inferred from the shape of the particle-hole continuum, whose shape will tend to be followed by the excitonic energies in the assumption that the binding energies do not depend too strongly on the total exciton momentum. In Ref. [21] we asserted that a Bernevig–Hughes–Zhang model with a band inversion for the underlying electrons comprises a promising candidate system with this feature. Furthermore, the qualitative conclusions of our work regarding inhomogeneous and supersolid phases of excitons are not strictly limited to a moat: as long as the excitonic energy landscape contains two or more degenerate minima the system will be in the regime susceptible to periodic order. In view of the general nature of our proposal, its potential as a new pathway to the realization of correlated excitonic phases, and the current rise of highly tunable electron–hole bilayers and related 2D material platforms, we hope that our work will inspire experimental efforts toward the realization of correlated excitonic phases.

## IX. ACKNOWLEDGMENTS

This work is supported by the Delta-ITP consortium, which is part of the Netherlands Organisation for Scientific Research (NWO). We also acknowledge the research program ‘‘Materials for the Quantum Age’’ (QuMat) for financial support. This program (registration number 024.005.006) is part of the Gravitation program financed by the Dutch Ministry of Education, Culture and Science (OCW).

### Appendix A: Equivalence between $T$ -matrix theory and short-range correlations

In this appendix we show that renormalizing the effective interaction in such a way that it is softened at the origin is equivalent to incorporating the effect of short-range correlations into the many-body wave function. Let us start with a more refined ansatz for the latter, namely

$$\Psi(\{\mathbf{r}_i\}) = \prod_i \psi(\mathbf{r}_i) \prod_{i \neq j} f(r_{ij}), \quad (\text{A1})$$

where  $r_{ij} \equiv |\mathbf{r}_i - \mathbf{r}_j|$ . Here,  $f(r_{ij})$  is a Jastrow factor which goes to zero when  $r_{ij} \rightarrow 0$  and assumes a value of one when  $r_{ij}$  exceeds some correlation distance [71]. Written in this way, the wave function becomes a product of single-particle wave functions when the interparticle distances are large enough, but vanishes when any two particles come too close to each other. Thus, we are effectively introducing the desired effect of short-range correlations into the variational ansatz.

Let us now calculate the interaction energy associated with this ansatz. This will have  $N(N-1)/2$  equal terms given by

$$\int d^d r_1 d^d r_2 |\psi(\mathbf{r}_1)|^2 V_{\text{eff}}(\mathbf{r}_1, \mathbf{r}_2) |\psi(\mathbf{r}_2)|^2, \quad (\text{A2})$$

where the effective interaction reads

$$V_{\text{eff}}(\mathbf{r}_1, \mathbf{r}_2) = V(\mathbf{r}_{12}) |f(\mathbf{r}_{12})|^2 \int d^d r_3 \dots d^d r_N \times \prod_{i>2} |\psi(\mathbf{r}_i)|^2 |f(\mathbf{r}_{1i})|^2 |f(\mathbf{r}_{2i})|^2 \prod_{i>j>2} |f(\mathbf{r}_{ij})|^2. \quad (\text{A3})$$

If the correlation distance is relatively small, then the integrals of the terms in the second line will be close to unity, so their role is to slightly renormalize the interaction strength of  $V$ . The most important effect is that  $V$  is now accompanied by the square of the Jastrow factor, as seen in the first line. Now, assuming that  $f$  does not vary too fast, its derivative can be neglected in the kinetic term. In this way, the resulting GPE for the single-particle wave function is the same as that obtained with the simpler ansatz  $\Psi(\{\mathbf{r}_i\}) = \prod_i \psi(\mathbf{r}_i)$ , except that the interaction potential  $V$  is replaced by  $V_{\text{eff}}$ , which modifies its behavior at the origin. Ultimately, the many-body  $T$  matrix turns out to be a suitable choice for this effective potential, as it precisely softens the short-range behavior of the bare interaction.

### Appendix B: $T$ -matrix formulation for a general BEC

In Sec. III A we have presented self-consistent equations for the FF, LO, and triangle phases taking into account the full microscopic renormalization of the bare interaction via the  $T$  matrix. In this Appendix we derive similar equations for a general coherent-state ansatz

$$|\Psi\rangle = \frac{1}{\sqrt{N!}} \left( \sum_{\mathbf{g}} c_{\mathbf{g}} b_{\mathbf{g}}^\dagger \right)^N |\emptyset\rangle, \quad (\text{B1})$$

which contains an arbitrary number of momenta. In the thermodynamic limit, the energy per particle of this state reads

$$\frac{\tilde{E}[\Psi]}{N} = \sum_{\tilde{\mathbf{g}}} |c_{\tilde{\mathbf{g}}}|^2 \tilde{\epsilon}_{\tilde{\mathbf{g}}} + \rho^2 \gamma \sum_{\{\tilde{\mathbf{g}}_i\}} c_{\tilde{\mathbf{g}}_1}^* c_{\tilde{\mathbf{g}}_2}^* c_{\tilde{\mathbf{g}}_3} c_{\tilde{\mathbf{g}}_1 + \tilde{\mathbf{g}}_2 - \tilde{\mathbf{g}}_3} \times t_{\frac{\tilde{\mathbf{g}}_1 - \tilde{\mathbf{g}}_2}{2}, \frac{\tilde{\mathbf{g}}_1 + \tilde{\mathbf{g}}_2}{2} - \tilde{\mathbf{g}}_3} (\tilde{\mathbf{g}}_1 + \tilde{\mathbf{g}}_2, -2\tilde{\mu}). \quad (\text{B2})$$

It is easy to check that this expression reproduces the energies of the FF and LO phases of the main text if only the coefficients  $c_{\mathbf{g}}$  and  $c_{\pm\mathbf{g}}$  are allowed to be nonzero, respectively. From Eq. (B2), together with the constraint  $\sum_{\tilde{\mathbf{g}}} |c_{\tilde{\mathbf{g}}}|^2 = 1$ , one easily derives the self-consistent equation

$$\tilde{\mu} c_{\tilde{\mathbf{g}}} = \tilde{\epsilon}_{\tilde{\mathbf{g}}} c_{\tilde{\mathbf{g}}} + \Lambda \sum_{\tilde{\mathbf{g}}', \tilde{\mathbf{g}}''} t_{\frac{\tilde{\mathbf{g}} - \tilde{\mathbf{g}}'}{2}, \frac{\tilde{\mathbf{g}} + \tilde{\mathbf{g}}'}{2} - \tilde{\mathbf{g}}''} (\tilde{\mathbf{g}} + \tilde{\mathbf{g}}', -2\tilde{\mu}) c_{\tilde{\mathbf{g}}'}^* c_{\tilde{\mathbf{g}}''} c_{\tilde{\mathbf{g}} + \tilde{\mathbf{g}}' - \tilde{\mathbf{g}}''}, \quad (\text{B3})$$

where we have used the fact that  $T_{\mathbf{k}\mathbf{k}'}(\mathbf{K}, E) = T_{-\mathbf{k}, -\mathbf{k}'}(\mathbf{K}, E)$  when the bare interaction is a function of  $|\mathbf{k} - \mathbf{k}'|$ . If the coherent state is assumed to correspond to a lattice solution, one can also minimize the energy with respect to the lengths of the reciprocal lattice basis vectors to yield additional self-consistent equations corresponding to the analogues of Eqs.

(11b) and (15b) for these higher-order lattices. Furthermore, in the case of a lattice solution one can connect with the Gross-Pitaevskii treatment and the corresponding Eq. (45), which assumes Bloch's theorem. This is accomplished by redefining  $\mathbf{g} \rightarrow \mathbf{g} + \mathbf{G}$  and  $c_{\mathbf{g}+\mathbf{G}} \equiv u_{\mathbf{g}\mathbf{G}}$ , where now  $\mathbf{G}$  is a reciprocal lattice vector and  $\mathbf{g}$  lies in the first Brillouin zone of the emerging reciprocal space, and simultaneously approximating  $t_{\mathbf{k}\mathbf{k}'}(\mathbf{K}, E)$  by a local, energy-independent function  $t_{\mathbf{k}-\mathbf{k}'}$ .

In Sec. III A we have briefly discussed the possibility of a hybrid zero-momentum-LO phase given by the state  $|\Psi_{\text{HLO}}\rangle$  of Eq. (16). Its free energy follows directly from Eq. (B2). In this case, the energy depends on the relative phase between the coefficients  $c_0$  and  $c_{\mathbf{g}}$ . Without loss of generality we choose  $c_{\mathbf{g}}$  as real, whence it is easy to show that the most optimal choice for the zero-momentum component is  $c_0 = i|c_0|$ , i.e.,  $c_0$  is purely imaginary. We can then verify if an infinitesimal  $c_0$  is able to develop from the LO phase anywhere on the parameter space of Fig. 2. To lowest order in  $c_0$ , the energy difference between the hybrid phase and the LO phase is given by  $(\tilde{E}^{(\text{HLO})} - \tilde{E}^{(\text{LO})})/N = \Delta|c_0|^2$ , where

$$\Delta \equiv \tilde{\epsilon}_m - \tilde{\mu}_{\text{LO}} + \Lambda \left[ t_{\frac{\tilde{\mathbf{g}}}{2}, \frac{\tilde{\mathbf{g}}}{2}}(\tilde{\mathbf{g}}, -2\tilde{\mu}_{\text{LO}}) + t_{\frac{\tilde{\mathbf{g}}}{2}, -\frac{\tilde{\mathbf{g}}}{2}}(\tilde{\mathbf{g}}, -2\tilde{\mu}_{\text{LO}}) - t_{\tilde{\mathbf{g}}, 0}(\tilde{\mathbf{g}}, -2\tilde{\mu}_{\text{LO}}) \right]. \quad (\text{B4})$$

Numerically we find that  $\Delta$  is positive everywhere, thus the LO phase remains pure in the entire region depicted in Fig. 3.

### Appendix C: Numerical treatment of the $T$ matrix

Here we outline our numerical procedure to obtain the full  $T$  matrix required for the plots of Figure 2. To efficiently compute the  $T$  matrix numerically, we expand the kernel in partial waves as

$$t_{\tilde{\mathbf{k}}\tilde{\mathbf{k}}'}(\tilde{\mathbf{K}}, \tilde{E}) = \sum_{mm'} t_{mm'}(\tilde{\mathbf{k}}, \tilde{\mathbf{k}}', \tilde{\mathbf{K}}, \tilde{E}) \frac{e^{im\phi_{\tilde{\mathbf{k}}}}}{\sqrt{2\pi}} \frac{e^{-im'\phi_{\tilde{\mathbf{k}}'}}}{\sqrt{2\pi}}. \quad (\text{C1})$$

Here we have set  $\phi_{\mathbf{K}} = 0$  without loss of generality for the rotationally invariant system, but we note that if the effects of warping are explicitly included in the single-particle dispersion, then  $\phi_{\mathbf{K}}$  must be chosen in the direction of one of the minima. The coefficients  $t_{mm'}$  then satisfy the coupled equations

$$t_{mm'}(\tilde{\mathbf{k}}, \tilde{\mathbf{k}}', \tilde{\mathbf{K}}, \tilde{E}) = \delta_{mm'} \sqrt{2\pi} v_m(\tilde{\mathbf{k}}, \tilde{\mathbf{k}}') + \int_0^\infty \frac{\tilde{p} d\tilde{p}}{(2\pi)^2} \sum_l v_m(\tilde{\mathbf{k}}, \tilde{\mathbf{p}}) g_{m-l}^{(2)}(\tilde{\mathbf{p}}, \tilde{\mathbf{K}}, \tilde{E}) t_{lm'}(\tilde{\mathbf{p}}, \tilde{\mathbf{k}}', \tilde{\mathbf{K}}, \tilde{E}), \quad (\text{C2})$$

where the angular components of the bare interaction and the two-boson propagator respectively read

$$v_m(\tilde{\mathbf{k}}, \tilde{\mathbf{k}}') = \int_0^{2\pi} \frac{d\phi}{\sqrt{2\pi}} v \sqrt{\tilde{k}^2 + \tilde{k}'^2 - 2\tilde{k}\tilde{k}' \cos \phi} e^{-im\phi}, \quad (\text{C3})$$

$$g_m^{(2)}(\tilde{\mathbf{p}}, \tilde{\mathbf{K}}, \tilde{E}) = \int_0^{2\pi} \frac{d\phi_{\tilde{\mathbf{p}}}}{\sqrt{2\pi}} \frac{e^{-im\phi_{\tilde{\mathbf{p}}}}}{\tilde{E} - \tilde{\epsilon}_{\tilde{\mathbf{K}}\hat{\mathbf{x}}/2+\tilde{\mathbf{p}}} - \tilde{\epsilon}_{\tilde{\mathbf{K}}\hat{\mathbf{x}}/2-\tilde{\mathbf{p}}}}. \quad (\text{C4})$$

We then solve the coupled set of equations (C2) by keeping partial waves with  $|m| \leq 4$  and discretizing the momentum space with  $N_{\tilde{\mathbf{k}}} = 1000$  points while imposing a momentum cutoff  $\tilde{k}_{\text{max}} = \max(10, 3\tilde{q}_m + 1)$  to correctly resolve the infrared features of both the dispersion and the bare interaction. We have checked that these parameters ensure convergence in all our calculations.

### Appendix D: Interaction energy of the chiral spin liquid

The interaction energy of the CSL state in the fully filled  $l$ th LL can be expressed as [72, 73]

$$\frac{E_{\text{int}}^{(l)}}{N} = \frac{n}{2} \int d^2r V(r) g_l(r) \quad (\text{D1a})$$

$$= \frac{n}{2} \int d^2r V(r) - \frac{1}{2} \int \frac{d^2q}{(2\pi)^2} V_{\mathbf{q}} |\mathcal{F}_l(q)|^2. \quad (\text{D1b})$$

In the first line we have written it in terms of the pair-correlation function  $g_l(r)$  corresponding to the fully filled LLL, while the expression in the second line involves the form factor

$$\mathcal{F}_l(q) = L_l \left( \frac{q^2 \ell_n^2}{2} \right) e^{-q^2 \ell_n^2 / 4}, \quad (\text{D2})$$

with  $L_l(x)$  the  $l$ th order Laguerre polynomial. In order to correctly compare with the FF phase it is important to keep the zero-momentum component of  $V$  corresponding to the first term of Eq. (D1b), as the calculation of the CSL correlation energy is performed with the bare interaction, while that of the BEC phases requires the associated  $T$  matrix, whose zero-point energy is in general slightly different. We note that our expression in Eq. (D1a) involves  $g_l(r)$  only, not the combination  $g_l(r) - 1$  like in the usual theory for the electronic QHE. This is because for excitons we do not need to subtract any neutralizing background, as the system is already charge-neutral and the interaction is integrable. In order to use the the LL form-factor formalism however, we must recall that the latter is derived by including the  $-1$  term, so that expression (D1b) results in our case. It can be easily shown for the  $l = 0$  case that both expressions lead to the same correlation energy by using the analytically known form factor

$$g_{l=0}(r) = 1 - e^{-r^2/2\ell_n^2}, \quad (\text{D3})$$

where  $\ell_n \equiv (2\pi n)^{-1/2}$  is the magnetic length. Either expression results in Eq. (24) of the main text. for the bilayer interaction of Eq. (8). The first term gives the zero-point energy  $(n/2) \int d^2r V(r)$ , while the second term corresponds to

the actual correlation energy of the usual QHE. In general, if the density is exactly  $\rho_l \equiv -\lambda/2(2l+1)$  so that the kinetic energy is perfectly quenched, the interaction energy in the case of the bilayer potential is given by

$$\frac{\tilde{E}_{\text{int}}^{(l)}}{N} = \rho_l^2 \gamma - \rho_l \gamma \int_0^\infty \frac{du}{2\sqrt{u}} (1 - e^{-2\rho_l \sqrt{u}}) [L_l(u)]^2 e^{-u}. \quad (\text{D4})$$

For small  $\rho_l$ , this gives

$$\frac{\tilde{E}_{\text{int}}^{(l)}}{N} \approx -\frac{\rho_l^3 \gamma}{\pi} \sum_{k=0}^l \frac{\Gamma(k-1/2)\Gamma(l+3/2-k)^2}{k![(l-k)!]^2}, \quad (\text{D5})$$

where the  $\rho_l^2$  term cancels because  $\int_0^\infty dx [L_l(x)]^2 e^{-x} = 1$ . Eq. (D5) shows that, in the case of a perfectly degenerate moat, the CSL will always have a lower energy than the BEC phases at small densities, as  $\tilde{E}_{\text{int}}^{(\text{CSL})} \propto \rho^3$  while  $\tilde{E}_{\text{int}}^{(\text{FF})} \propto \rho^2$ . Furthermore, the rightmost LL is that with  $l=0$ , so there is a maximum value of  $\rho$  for which the LL energy can be nullified and above which the BEC phases can become stable. In practice, as explained in Sec. III D, band-structure warping in real systems will likely destabilize the CSL phase in a large region of the parameter space.

- 
- [1] J. Eisenstein and A. H. MacDonald, Bose–Einstein condensation of excitons in bilayer electron systems, *Nature* **432**, 691 (2004).
- [2] J. Eisenstein, Exciton condensation in bilayer quantum Hall systems, *Annu. Rev. Condens. Matter Phys.* **5**, 159 (2014).
- [3] N. J. Zhang, R. Q. Nguyen, N. Batra, X. Liu, K. Watanabe, T. Taniguchi, D. Feldman, and J. Li, Excitons in the fractional quantum Hall effect, *Nature* **637**, 327 (2025).
- [4] S. Brem, C. Linderålv, P. Erhart, and E. Malic, Tunable phases of moiré excitons in van der Waals heterostructures, *Nano Letters* **20**, 8534 (2020).
- [5] N. P. Wilson, W. Yao, J. Shan, and X. Xu, Excitons and emergent quantum phenomena in stacked 2D semiconductors, *Nature* **599**, 383 (2021).
- [6] E. C. Regan, D. Wang, E. Y. Paik, Y. Zeng, L. Zhang, J. Zhu, A. H. MacDonald, H. Deng, and F. Wang, Emerging exciton physics in transition metal dichalcogenide heterobilayers, *Nature Reviews Materials* **7**, 778 (2022).
- [7] B. H. Moon, A. Mondal, D. K. Efimkin, and Y. H. Lee, Exciton condensate in van der Waals layered materials, *Nature Reviews Physics* **7**, 388 (2025).
- [8] R. Qi, Q. Li, Z. Zhang, J. Nie, B. Zou, Z. Cui, H. Kim, C. Sanborn, S. Chen, J. Xie, *et al.*, Competition between excitonic insulators and quantum Hall states in correlated electron–hole bilayers, *Nature Materials*, 1 (2025).
- [9] J. Li, T. Taniguchi, K. Watanabe, J. Hone, and C. Dean, Excitonic superfluid phase in double bilayer graphene, *Nature Physics* **13**, 751 (2017).
- [10] J. Cutshall, F. Mahdikhany, A. Roche, D. N. Shanks, M. R. Koehler, D. G. Mandrus, T. Taniguchi, K. Watanabe, Q. Zhu, B. J. LeRoy, *et al.*, Imaging interlayer exciton superfluidity in a 2D semiconductor heterostructure, *Science Advances* **11**, eadr1772 (2025).
- [11] R. Xiong, J. H. Nie, S. L. Brantly, P. Hays, R. Sailus, K. Watanabe, T. Taniguchi, S. Tongay, and C. Jin, Correlated insulator of excitons in WSe<sub>2</sub>/WS<sub>2</sub> moiré superlattices, *Science* **380**, 860 (2023).
- [12] B. Gao, D. G. Suárez-Forero, S. Sarkar, T.-S. Huang, D. Session, M. J. Mehrabad, R. Ni, M. Xie, P. Upadhyay, J. Vannucci, *et al.*, Excitonic Mott insulator in a Bose-Fermi-Hubbard system of moiré WS<sub>2</sub>/WSe<sub>2</sub> heterobilayer, *Nature Communications* **15**, 2305 (2024).
- [13] Z. Lian, Y. Meng, L. Ma, I. Maity, L. Yan, Q. Wu, X. Huang, D. Chen, X. Chen, X. Chen, *et al.*, Valley-polarized excitonic Mott insulator in WS<sub>2</sub>/WSe<sub>2</sub> moiré superlattice, *Nature Physics* **20**, 34 (2024).
- [14] S. Miao, T. Wang, X. Huang, D. Chen, Z. Lian, C. Wang, M. Blei, T. Taniguchi, K. Watanabe, S. Tongay, *et al.*, Strong interaction between interlayer excitons and correlated electrons in WSe<sub>2</sub>/WS<sub>2</sub> moiré superlattice, *Nature communications* **12**, 3608 (2021).
- [15] L. Yan, L. Ma, Y. Meng, C. Xiao, B. Chen, Q. Wu, J. Cui, Q. Cao, R. Banerjee, T. Taniguchi, *et al.*, Anomalously enhanced diffusivity of moiré excitons via manipulating the interplay with correlated electrons, *Nature Communications* **16**, 10569 (2025).
- [16] A. Julku, Nonlocal interactions and supersolidity of moiré excitons, *Physical Review B* **106**, 035406 (2022).
- [17] T.-S. Huang, Y.-Z. Chou, C. L. Baldwin, F. Wu, and M. Hafezi, Mott-moiré excitons, *Physical Review B* **107**, 195151 (2023).
- [18] D. D. Dai and L. Fu, Strong-coupling phases of trions and excitons in electron-hole bilayers at commensurate densities, *Physical Review Letters* **132**, 196202 (2024).
- [19] P. Froese, T. Neupert, and G. Wagner, Topological excitons in moiré MoTe<sub>2</sub>/WSe<sub>2</sub> heterobilayers, *Physical Review Research* **7**, 023047 (2025).
- [20] J.-Y. You, C.-E. Hsu, Z. Zhu, B. Zhang, Z. Ye, M. H. Naik, T. Cao, H.-C. Hsueh, S. G. Louie, M. Del Ben, *et al.*, Moiré excitons in generalized Wigner crystals, arXiv preprint arXiv:2509.08211 (2025).
- [21] L. Maisel Licerán, F. García Flórez, L. D. Siebbeles, and H. T. Stoof, Single-particle properties of topological Wannier excitons in bismuth chalcogenide nanosheets, *Scientific Reports* **13**, 6337 (2023).
- [22] G. V. Chester, Speculations on Bose–Einstein condensation and quantum crystals, *Physical Review A* **2**, 256 (1970).
- [23] A. F. Andreev and I. M. Lifshitz, Quantum Theory of Defects in Crystals, *Soviet Journal of Experimental and Theoretical Physics* **29**, 1107 (1969).
- [24] A. J. Leggett, Can a solid be “superfluid”?, *Physical Review Letters* **25**, 1543 (1970).
- [25] S. Balibar, The enigma of supersolidity, *Nature* **464**, 176 (2010).
- [26] Y. N. Joglekar, A. V. Balatsky, and S. Das Sarma, Wigner supersolid of excitons in electron-hole bilayers, *Physical Review B—Condensed Matter and Materials Physics* **74**, 233302 (2006).
- [27] S. Conti, A. Perali, A. R. Hamilton, M. V. Milošević, F. M. Peeters, and D. Neilson, Chester supersolid of spatially indirect excitons in double-layer semiconductor heterostructures, *Physical Review Letters* **130**, 057001 (2023).

- [28] S. Conti, A. Chaves, A. R. Hamilton, J. Tempere, M. V. Milosevic, and D. Neilson, A Gross-Pitaevskii theory for an excitonic incompressible Bose solid, arXiv preprint arXiv:2507.20236 (2025).
- [29] J. de Oliveira Neto, F. Guimarães, D. S. Dantas, F. Peeters, M. Milošević, and A. Chaves, Striped excitonic (super) solid in anisotropic semiconductors with screened exciton interactions, *Physical Review B* **111**, L180506 (2025).
- [30] T. A. Sedrakyan, A. Kamenev, and L. I. Glazman, Composite fermion state of spin-orbit-coupled bosons, *Physical Review A* **86**, 063639 (2013).
- [31] T. A. Sedrakyan, L. I. Glazman, and A. Kamenev, Absence of Bose condensation on lattices with moat bands, *Physical Review B* **89**, 201112 (2014).
- [32] T. A. Sedrakyan, L. I. Glazman, and A. Kamenev, Spontaneous formation of a nonuniform chiral spin liquid in a moat-band lattice, *Physical Review Letters* **114**, 037203 (2015).
- [33] T. A. Sedrakyan, V. M. Galitski, and A. Kamenev, Statistical transmutation in Floquet driven optical lattices, *Physical Review Letters* **115**, 195301 (2015).
- [34] C. Wei and T. A. Sedrakyan, Chiral spin liquid state of strongly interacting bosons with a moat dispersion: A Monte Carlo simulation, *Annals of Physics* **456**, 169354 (2023).
- [35] M. Bijlsma and H. Stoof, Variational approach to the dilute Bose gas, *Physical Review A* **55**, 498 (1997).
- [36] N. Proukakis, S. Morgan, S. Choi, and K. Burnett, Comparison of gapless mean-field theories for trapped Bose-Einstein condensates, *Physical Review A* **58**, 2435 (1998).
- [37] M. D. Lee, S. A. Morgan, M. J. Davis, and K. Burnett, Energy-dependent scattering and the Gross–Pitaevskii equation in two-dimensional Bose–Einstein condensates, *Physical Review A* **65**, 043617 (2002).
- [38] C. Gies, M. Lee, and D. Hutchinson, Many-body  $t$ -matrix of a two-dimensional Bose–Einstein condensate within the Hartree–Fock–Bogoliubov formalism, *Journal of Physics B: Atomic, Molecular and Optical Physics* **38**, 1797 (2005).
- [39] H. T. C. Stoof and M. Bijlsma, Kosterlitz–Thouless transition in a dilute Bose gas, *Physical Review E* **47**, 939 (1993).
- [40] J. Andersen, U. Al Khawaja, and H. T. C. Stoof, Phase fluctuations in atomic Bose gases, *Physical Review Letters* **88**, 070407 (2002).
- [41] U. Al Khawaja, J. Andersen, N. Proukakis, and H. C. Stoof, Low dimensional bose gases, *Physical Review A* **66**, 013615 (2002).
- [42] K. Rajagopal, P. Vignolo, and M. Tosi, Density profile of a strictly two-dimensional Bose gas at finite temperature, *Physica B: Condensed Matter* **344**, 157 (2004).
- [43] In Ref. [37], a somewhat more detailed (but not fully rigorous) argument is used to justify that the 2D many-body  $T$  matrix should be replaced by the two-body one at an energy  $-\mu$ , as opposed to  $-2\mu$ . However, the calculation depends on the precise form of the single-particle dispersion and is therefore not universal. In view of this uncertainty we choose here to consider the  $-2\mu$  energy arising from the intuitive physical picture. In any case, we do not expect the results to be affected significantly by this particular aspect of the theory.
- [44] P. A. Noordman, L. Maisel Licerán, and H. T. Stoof, Variational and field-theoretical approach to exciton–exciton interactions and biexcitons in semiconductors, arXiv preprint arXiv:2510.05242 (2025).
- [45] N. Götzing, F. Lohof, and C. Gies, Moiré–Bose–Hubbard model for interlayer excitons in twisted transition metal dichalcogenide heterostructures, *Physical Review B* **105**, 165419 (2022).
- [46] P. Fulde and R. A. Ferrell, Superconductivity in a strong spin-exchange field, *Physical Review* **135**, A550 (1964).
- [47] A. I. Larkin and Y. N. Ovchinnikov, Inhomogeneous state of superconductors, *Sov. Phys. JETP* **20**, 762 (1965).
- [48] Note that here we follow the nomenclature of Refs. [? ? ] and make the distinction between the FF and LO phases, which are often collectively denoted as the “FFLO” phase in the literature. This distinction is important because only the LO state corresponds to a spatially inhomogeneous state, and furthermore their superfluid properties are completely different.
- [49] N. Sepúlveda, C. Josserand, and S. Rica, Nonclassical rotational inertia fraction in a one-dimensional model of a supersolid, *Physical Review B* **77**, 054513 (2008).
- [50] N. Sepulveda, C. Josserand, and S. Rica, Superfluid density in a two-dimensional model of supersolid, *The European Physical Journal B* **78**, 439 (2010).
- [51] K. Yang and S. Sachdev, Quantum criticality of a Fermi gas with a spherical dispersion minimum, *Physical Review Letters* **96**, 187001 (2006).
- [52] S. Gopalakrishnan, A. Lamacraft, and P. M. Goldbart, Universal phase structure of dilute Bose gases with Rashba spin-orbit coupling, *Physical Review A* **84**, 061604 (2011).
- [53] H. T. Stoof, K. B. Gubbels, and D. B. Dickerscheid, *Ultracold quantum fields* (Springer, 2009).
- [54] A. J. Leggett, *Quantum liquids: Bose condensation and Cooper pairing in condensed-matter systems* (Oxford University Press, 2006).
- [55] S. Maiti and T. Sedrakyan, Fermionization of bosons in a flat band, *Physical Review B* **99**, 174418 (2019).
- [56] S. C. Zhang, T. H. Hansson, and S. Kivelson, Effective-field-theory model for the fractional quantum Hall effect, *Physical Review Letters* **62**, 82 (1989).
- [57] A. Lopez and E. Fradkin, Fractional quantum Hall effect and Chern-Simons gauge theories, *Physical Review B* **44**, 5246 (1991).
- [58] S. C. Zhang, The Chern–Simons–Landau–Ginzburg theory of the fractional quantum Hall effect, *International Journal of Modern Physics B* **6**, 25 (1992).
- [59] L. Fu, Hexagonal warping effects in the surface states of the topological insulator  $\text{Bi}_2\text{Te}_3$ , *Physical Review Letters* **103**, 266801 (2009).
- [60] C.-X. Liu, X.-L. Qi, H. Zhang, X. Dai, Z. Fang, and S.-C. Zhang, Model Hamiltonian for topological insulators, *Physical Review B* **82**, 045122 (2010).
- [61] S. Brazovskii, Phase transition of an isotropic system to a nonuniform state, in *30 Years Of The Landau Institute—Selected Papers* (World Scientific, 1996) pp. 109–113.
- [62] F. Rabec, G. Brochier, S. Wattellier, G. Chauveau, Y. Li, S. Nascimbene, J. Dalibard, and J. Beugnon, Superfluid fraction of a 2D Bose-Einstein condensate in a triangular lattice, arXiv preprint arXiv:2511.04575 (2025).
- [63] Note that Leggett’s bound in the form given here does not universally apply to the moat-band case due to the mixing of the ordering vectors and the components of the phase gradient in Eq. (29). However, for the LO phase in particular, the derived expression coincides with the one by Leggett as  $n(\mathbf{r}) \propto \cos^2 q_m \cdot x$ .
- [64] L. De Goeij, T. van den Berg, N. Mulders, H. Stoof, B. Verhaar, and W. Glöckle, Three-body recombination in spin-polarized atomic hydrogen, *Physical Review B* **34**, 6183 (1986).
- [65] The reason for writing  $\tilde{g}_1$  and  $-\tilde{g}_2$  as  $\pm\tilde{G}/2$  is that in our numerical procedure we obtain the order parameter as  $\phi(x) = e^{igx}(u_0 + u_1 e^{iGx})$ , where  $g = -G/2$  lies in the first Brillouin zone. In this way, the Bloch factor is identified with the term inside parentheses, which has the same periodicity as the emerging density lattice. Because in the Landau theory we group  $g$  and  $G$  together, ultimately  $g_1$  and  $g_2$  must be identified with

- $\pm G/2$  in order to compare with the numerical result.
- [66] Writing the coefficients as  $u_i = |u_i|z_i$ , where  $|z_i| = 1$ , an optimal choice for the phases is  $z_i = 1$  for all  $i$  when  $t_{\bar{q}_m} + t_{\sqrt{3}\bar{q}_m} < 0$ , and  $z_1z_4 = 1$ ,  $z_2z_5 = e^{2i\pi/3}$ ,  $z_3z_6 = e^{4i\pi/3}$  when  $t_{\bar{q}_m} + t_{\sqrt{3}\bar{q}_m} > 0$ . This choice lead to the expressions of Eq. (56).
- [67] S. Mkhonta, K. Elder, and Z.-F. Huang, Exploring the complex world of two-dimensional ordering with three modes, *Physical Review Letters* **111**, 035501 (2013).
- [68] V. Heinonen, K. J. Burns, and J. Dunkel, Quantum hydrodynamics for supersolid crystals and quasicrystals, *Physical Review A* **99**, 063621 (2019).
- [69] A. Mendoza-Coto, R. Turcati, V. Zampronio, R. Díaz-Méndez, T. Macrì, and F. Cinti, Exploring quantum quasicrystal patterns: A variational study, *Physical Review B* **105**, 134521 (2022).
- [70] M. Grossklags, M. Ciardi, V. Zampronio, F. Cinti, and A. Mendoza-Coto, Self-induced Bose glass phase in quantum quasicrystals, *Results in Physics* **65**, 107991 (2024).
- [71] R. Jastrow, Many-body problem with strong forces, *Physical Review* **98**, 1479 (1955).
- [72] S. M. Girvin, The quantum Hall effect: Novel excitations and broken symmetries, in *Aspects topologiques de la physique en basse dimension. Topological aspects of low dimensional systems: Session LXIX. 7–31 July 1998* (Springer, 2002) pp. 53–175.
- [73] I. Sodemann and A. MacDonald, Landau level mixing and the fractional quantum Hall effect, *Physical Review B* **87**, 245425 (2013).